Journal of Geodynamics 121 (2018) 155–184

Contents lists available at ScienceDirect

Journal of Geodynamics

journal homepage: www.elsevier.com/locate/jog

Tectonics of the New Siberian Islands archipelago: Structural styles and low-temperature thermochronology

Andrei V. Prokopiev[a,*], Victoria B. Ershova[b], Owen Anfinson[c,d], Daniel Stockli[c], Jeremy Powell[e], Andrei K. Khudoley[b], Dmitry A. Vasiliev[a], Nikolay N. Sobolev[f], Eugeny O. Petrov[f]

[a] Diamond and Precious Metal Geology Institute, Siberian Branch, Russian Academy of Sciences, Lenin Prospect 39, Yakutsk, 677980, Russia
[b] Institute of Earth Science, St. Petersburg State University, Universitetskaya nab. 7/9, Saint Petersburg, 199034, Russia
[c] Jackson School of Geoscience, University of Texas at Austin, USA
[d] Sonoma State University, Department of Geology, USA
[e] Natural Resources Canada, Geological Survey of Canada, 601 Booth St., Ottawa, ON, K1a OE9, Canada
[f] All Russian Geological Institute (VSEGEI), Sredniy Prospect 74, Saint Petersburg, 199106, Russia

ARTICLE INFO

Keywords:
Tectonics
Structural analysis
Low-temperature thermochronology
New Siberian Islands
Arctic

ABSTRACT

Tectonic evolution of the New Siberian Islands (NSI) has been revealed based on detailed structural investigations and a (U-Th)/He low-temperature thermochronologic study of detrital zircons (ZHe) and apatite (AHe). Our study supports models claiming a non–Siberian affinity of the NSI and furthermore suggests that the study area formed a part of the Arctic-Alaska-Chukotka microcontinent. Seven stages of deformation have been revealed. The earliest stage (Stage 1) involved contractional deformation with transport directions towards the W-to WSW and occurred during the Late Cambrian across the De Long Islands. The next episode of deformation (Stage 2) has been revealed based on the low-temperature thermochronology (ca. 378–414 Ma, ZHe) and structural data. A pre-Frasnian angular unconformity formed as a result of Stage 2 deformation on Kotel'nyi Island, which involved contractional deformation with S-to SW transport directions (modern coordinates) in the mid-Paleozoic. In the latest Early Cretaceous–Late Cretaceous, three deformation stages were initiated by collision between the western part of the Arctic-Alaska-Chukotka microcontinent and Siberia, forming the South Anyui suture zone and overlapping orogenic belt. Stage 3 was characterized by the formation of major NW-trending folds, thrusts, and both transfer dextral and sinistral strike-slip faults with a reverse component. During Stage 4, the Arctic Alaska-Chukotka microcontinent moved westward. On Bolshoy Lyakhovsky Island, sinistral strike-slip faults were formed, whilst E-W compression took place across the Anjou islands. In Stage 5, the Arctic Alaska-Chukotka microcontinent shifted southward, forming a series of N-S-trending dextral strike-slip faults. The ZHe and AHe ages (ca. 93–125 Ma) suggest that these deformation events were associated with significant uplift in the western part of the NSI (Kotel'nyi and Bel'kovsky islands), whilst the eastern part (De Long Islands) was marginally affected by these events without significant uplift. The Cenozoic extension event (Stage 6) corresponds to the opening of the Eurasian Basin. This stage is manifested by the cooling episode (ca. 53 Ma, Early Eocene, AHe) established in the eastern part of the NSI (Jeannette Island). The origins of the late Cenozoic contractional deformations described from the Cenozoic deposits of the Anjou Islands (Stage 7) are unclear, but were possibly caused by movements along the Eurasian and North-American lithospheric plates.

1. Introduction

The New Siberian Islands (NSI) archipelago is located in the eastern part of the Russian High Arctic at the boundary between the Laptev and East Siberian seas. It consists of three island groups: the Anjou, De Long and Lyakhovsky Islands (Fig. 1). The NSI were extensively studied 30–40 years ago by Kos'ko et al. (1985), when the first geological maps were compiled. In the Anjou, Lyakhovsky, and two islands of the De Long group (Bennett and Henrietta islands), the general strike of structures and location of the main unconformities were established, major faults were mapped, and their kinematics determined. More recently, the Anjou and Lyakhovsky Islands were visited, which comprise the largest islands within the archipelago with the most extensive rock exposures available to study (Brandes et al., 2015; Drachev, 1999,

* Corresponding author.
E-mail address: prokopiev@diamond.ysn.ru (A.V. Prokopiev).

https://doi.org/10.1016/j.jog.2018.09.001
Received 15 August 2017; Received in revised form 22 July 2018; Accepted 2 September 2018
Available online 05 September 2018
0264-3707/

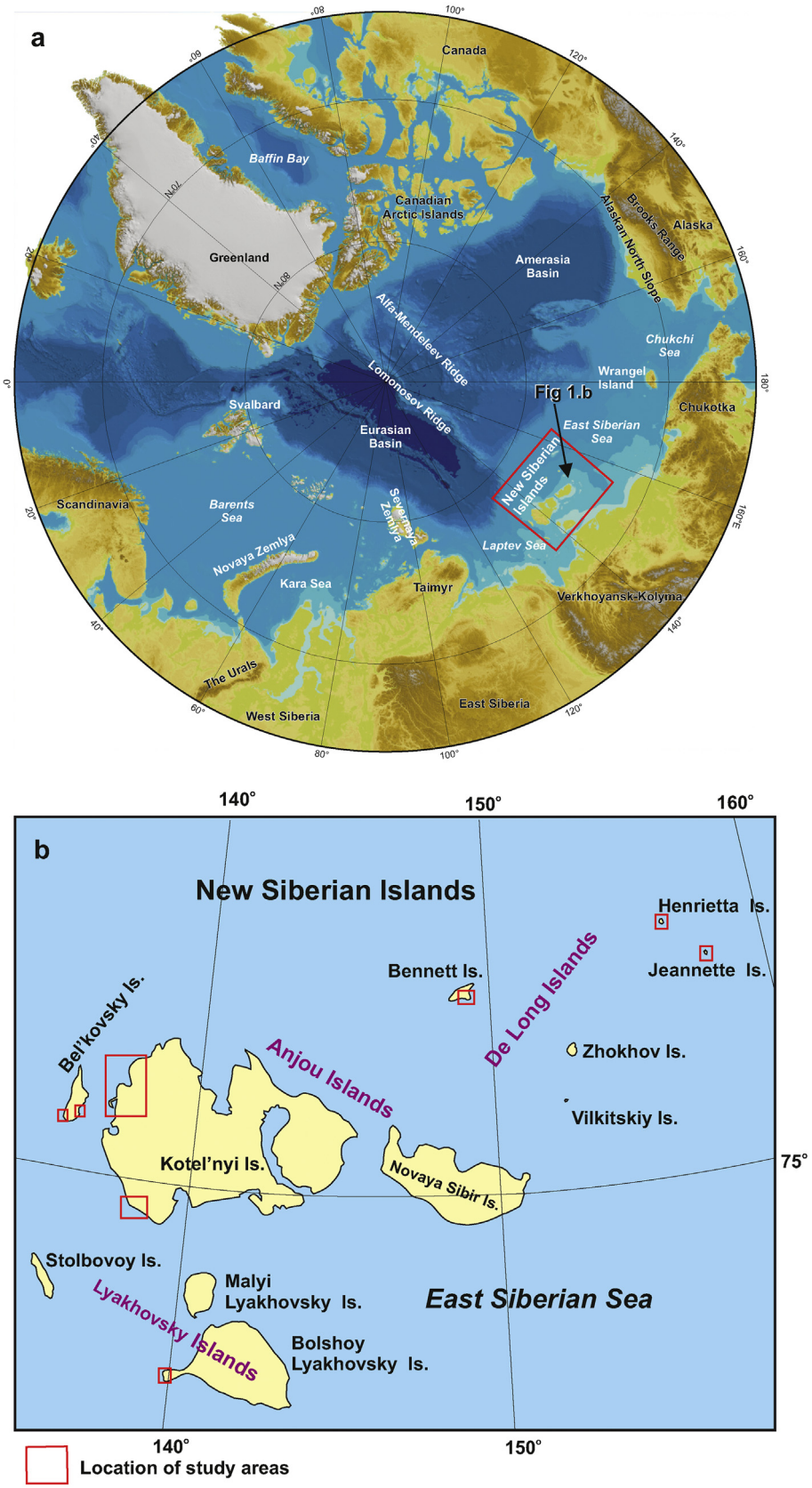

Fig. 1. (a) Regional setting of the study area; (b) sketch map of New Siberian Islands Archipelago showing studied locations (red rectangulars). (For interpretation of the references to colour in this figure legend, the reader is referred to the web version of this article.)

2002, Drachev et al., 2011; Drachev, 2016; Drachev et al., 1998; Ershova et al., 2015a,b,2016b; Kos'ko and Trufanov, 2002; Kuzmichev, 2009; Piepjohn et al., 2017 and references therein). By contrast, comparatively few studies have focused on the small De Long Island group, and many aspects of their geological history are still unknown or remain a matter of debate (e.g. Chernova et al., 2017; Ershova et al., 2016a; Matushkin et al., 2016; Sobolev et al., 2014 and references therein).

Several contrasting paleotectonic reconstructions have been proposed for the affinity of the NSI. For example, Kuzmichev (2009) and Danukalova (2016) suggested that the NSI were part of the Siberian paleocontinent, whereas Zonenshain et al. (1990) argued that the NSI formed a portion of the Arctida paleocontinent, which shared an affinity with Laurentia until the late Mesozoic. The paleomagnetic study of Vernikovsky et al. (2013) showed the differing apparent polar wander paths of the NSI and Siberia, while Metelkin et al. (2014, 2015) proposed that the NSI were a separate terrane in Paleozoic times but linked to the Kolyma-Omolon microcontinent (superterrane) in Mesozoic times. Recent detrital zircon studies of the Paleozoic succession on the NSI suggest an affinity with Laurentia or Baltica (Ershova et al., 2015a,b, 2016a,b).

At the present time, the NSI are mainly considered as part of the New Siberian-Chukotka, New Siberian-Chukotka-North Alaska, Chukotka-Alaska or Arctic Alaska-Chukotka microcontinents (superterranes, microplates) or the Arctida and Bennett-Barovia terranes (e.g. Grantz et al., 1990; Lawver et al., 2002; Miller et al., 2006; Natal'in et al., 1999; Nokleberg et al., 2001; Sengo¨r and Natal'in, 1996; Vernikovsky et al., 2013 and references therein). It is assumed that the Arctic Alaska-Chukotka microcontinent was separated by the South Anyui/Angayucham Ocean from Siberia in the late Paleozoic and accreted to northeast Asia in late Mesozoic time. However, the location and continuation of the South Anyui Suture Zone from the mainland of Siberia towards the New Siberian Islands and/or Laptev Sea is open to discussion (e.g. Brandes et al., 2015; Drachev et al., 2011; Franke et al., 2008; Kuzmichev, 2009; Metelkin et al., 2014, 2015; Piepjohn et al., 2017 and references therein).

Structural geology investigations in the islands have been very limited to date. Verzhbitsky (2004, 2009) defined the sequence of deformation structures on the western Bel'kovsky Island. Brandes et al. (2015) carried out palaeo-stress field analysis and determined the principle palaeo-shortening and palaeo-extension directions, proposing a Meso-Cenozoic structural evolution. Piepjohn et al. (2017) have carried out structural analyses across most of the NSI, and they have proposed a succession of structural events and a possible explanation for the continuation of the South Anyui Suture Zone to the west. Both Piepjohn et al. (2017) and Shephard et al. (2013) supposed the existence of a transform fault along the margin of the Lomonosov Ridge, along which the Arctic Alaska–Chukotka microcontinent moved relative to the Eurasian margin.

However, many questions remain unresolved, including the sequence and timing of deformations, particularly those of the pre-Mesozoic, their correlation within the archipelago, and relation to geodynamic events manifested in this part of the Arctic. The principle aim of this paper is to fill in these critical gaps in geological knowledge and present data and interpretations obtained from three expeditions to the NSI carried out during the summers of 2012, 2013 and 2014. Here we present new data on the structural geology and low-temperature thermochronology across Kotel'nyi and Bel'kovsky islands (Anjou Islands), Henrietta, Jeannette and Bennett islands (De Long Islands), and Bolshoy Lyakhovsky Island (Lyakhovsky Islands).

Our primary objectives were to: (1) study the structural geology to define the sequence of tectonic deformations, (2) carry out a (U-Th)/He low-temperature thermochronologic study of detrital zircons (ZHe) and apatite (AHe) to determine the age of the uplifts and associated tectonic events.

2. Structural geology and low-temperature thermochronology

2.1. Methods

2.1.1. Structural studies

The detailed structural studies have been conducted on six islands of the NSI archipelago. During fieldwork we identified structural associations formed during different deformational stages according to their cross-cutting relationships, and carried out measurements of bedding, cleavage, bedding-cleavage intersection lineation, and other structural elements. These measurements were plotted up using the StereoNett software. The orientation of striae on the slickensides were interpreted based on approaches presented by Marrett and Allmendinger (1990) and Allmendinger et al. (2012) using FaultKinWin software. In the text below, we call σ_1, σ_2 and σ_3 as tension, intermediate and compression axes respectively. All stereonets are equal-area (Schmidt) diagrams, with a lower hemisphere projection. Deformation stages and associated structural elements were separately identified on each island. For their designations, the first letters of the names of islands were used in the upper case: J – Jeannette, H – Henrietta, B – Bennett, K – Kotel'nyi, Bl – Bel'kovsky islands and L – Bolshoy Lyakhovsky islands. For example for Jeannette island we have distinguished the following deformation stages: $D^J_{1...3}$, $F^J_{1...2}$, S^J_1. The correlation of deformation stages observed across the studied islands is presented in the Discussion.

2.1.2. Low-temperature thermochronology

2.1.2.1. (U-Th)/He dating. (U-Th)/He detrital zircon and apatite analyses were performed on 12 samples within the NSI. Samples were crushed and the heavy minerals were concentrated using standard techniques at the Institute of Precambrian Geology and Geochronology, Russian Academy of Science. (U–Th)/He dating of detrital zircons and apatite was carried out at the UTChron geochronology facility in the Department of Geosciences at the University of Texas at Austin.

Apatite and zircon (U-Th)/He thermochronology measures radiogenic ^{4}He produced during the decay of ^{238}U, ^{235}U, ^{232}Th and ^{147}Sm. Diffusion of helium in apatite and zircon is thermally controlled, occurring readily at high temperatures. These minerals become increasingly retentive of radiogenic helium as they cool through low-temperatures in the uppermost crust (Harrison and Zeitler, 2005). Although many studies invoke closure temperatures of ~70 °C (Farley, 2000) and ~185 °C (Reiners et al., 2002; Wolfe and Stockli, 2010) for the AHe and ZHe systems, respectively, this concept requires a monotonic cooling history from open to closed system (Reiners and Brandon, 2006). As a result, the closure temperature concept, and the idea of an AHe or ZHe cooling age, is not of much use when applied to thermochronology of sedimentary basins. In these environments, strata typically reside for long durations at temperatures below 200 °C, in which apatite and zircon may be partially retentive of radiogenic helium.

In addition to cooling rates, grain size and radiation damage also control diffusion kinetics of helium in apatite and zircon (Farley, 2002). In apatite, the accumulation of radiation damage in the crystal structure results in an AHe system that is increasingly retentive of radiogenic helium (Flowers et al., 2009; Gautheron et al., 2009; Shuster et al., 2006). In the ZHe system, zircon becomes more retentive of helium with increasing radiation damage, until a threshold amount of damage is reached. Beyond this threshold, progressive radiation damage to the crystal structure results in a substantial decrease in the retention of radiogenic helium (Guenthner et al., 2013). A relative proxy for radiation damage is the grain-specific effective uranium concentration ($eU = [U] + 0.235 \cdot [Th]$; Flowers et al., 2009), which is integrated over the time spent below temperatures corresponding with fission track annealing in apatite and zircon (Flowers et al., 2009; Guenthner et al., 2013) to assess the effect of damage accumulation on helium diffusion. Since apatite fission track annealing kinetics vary with composition (Barbarand et al., 2003; Carlson et al., 1999; Green et al., 1986), apatite chemistry must be understood in order to quantify

relationships between AHe dates and eU (Gautheron et al., 2013). Interpretation of AHe and ZHe dates from sedimentary rocks is complicated due to intra-sample variability of grain size (Beucher et al., 2013; Brown et al., 2013), chemistry (Djimbi et al., 2015; Gautheron et al., 2013) and radiation damage, compounded with the effects of an unknown pre-depositional thermal history of the accessory minerals (Guenthner et al., 2015).

2.1.2.1.1. Thermal history modelling. In order to understand the implications of our apatite and zircon (U-Th)/He data for the thermal history of the NSI, we performed inverse and forward thermal history modelling using the software HeFTy (Ketcham, 2005; version 1.9.1). HeFTy uses a Monte Carlo approach to generate time-temperature paths through user specified time-temperature constraints, and then applies a combined merit function to assess the agreement between modeled and empirical data. Paths are deemed as "acceptable" or "good" should they meet certain statistical precision limits. Due to the limited understanding on burial and exhumation history of the NSI, our inverse models search for a single heating and cooling event from deposition to present day. For a given inverse model, we incorporate a subset of 2–4 AHe dates that span the range of observed AHe ages and eU concentrations for the sample, and model these dates with a 10% error. Next, we use forward modelling of discrete t-T histories that fall within the solution envelope to determine whether dispersion amongst AHe and ZHe dates can be accounted for by maximum burial temperatures and cooling histories indicated from inverse modelling. Forward models for apatite show the predicted AHe date-eU trends for standard fluorapatite (0.83 rmr0) as well as apatite chemistries that are more (< 0.4 rmr0) and less (< 0.9 rmr0) resistant to thermal annealing of radiation damage. Forward models for ZHe data plot the ZHe inheritance envelope (Guenthner et al., 2015), which encompasses the expected date-eU trends for a range of all possible pre-depositional histories from the maximum U-Pb date to a zero-inheritance depositional age (Ershova et al., 2016a).

All detrital zircon and apatite (U-Th)/He analytical results are provided in Attachment 1.

2.2. De Long Islands

2.2.1. Structural studies of Jeannette Island (southern part)

The Upper Cambrian volcaniclastic rocks (Ershova et al., 2016a) in the studied part of the island generally dip to the W-SW at angles of 40–70° (Fig. 2a, b). Folds F_1^J, varying in width from a few meters to a few tens of meters, are observed, often accompanied by the axial plane cleavage S_1^J, mostly dipping towards the east (Fig. 3a, b). The folds are associated with west-northwest-directed thrusts, thus confirming a general westward direction of tectonic transport. There are en-echelon-arranged quartz veins defining shear zones characterized by thrust kinematics (Fig. 3c). The cleavage and bedding intersection lineation L_1^J plunge southeastward at 5–15° (Fig. 2b). The rocks are metamorphosed to greenschist facies (Dorofeev et al., 1999). Chlorite and sericite occur on the cleavage planes, suggesting that the metamorphic event was related to first deformation stage (D_1^J). Late Cambrian dolerite dykes (497.23 ± 1 Ma, plagioclase, $^{40}Ar/^{39}Ar$) trend mainly to the WNW-ESE and locally NE-SW (Prokopiev et al., 2017), and intruded into both folded and undeformed strata (Fig. 3d). There are small-scale normal faults with fault planes inclined to the east (D_2^J), which displace deformed sedimentary rocks and late Cambrian dykes (Fig. 3e, f).

2.2.2. Structural studies of Henrietta Island

The island comprises Ediacaran (Unit A) and Cambrian (Unit B) volcaniclastic rocks (Ershova et al., 2016a) with similar structural styles. Unlike Jeannette Island, located ~ 50 km to the east, the rocks of Henrietta island are unmetamorphosed. Slickensides and cleavage planes have not been reported within the studied locations. The Ediacaran part of the succession (Unit A) is intruded by mafic dykes yielding ages of ca. 562 Ma (plagioclase, $^{40}Ar/^{39}Ar$, Prokopiev et al., 2017), trending mainly to the NW-SE (Fig. 4). The most intense deformation is found near Cape Sadko in the southwest of the island. Here, there are numerous thrusts of the first deformation stage (D_1^H) of different scales, characterized by west-directed transport and accompanied by NNW-SSE trending F_1^H–folds of different scales which are partly overturned to the WSW (Figs. 4c, 5 a–e). The fold axes are gently plunging (up to 15–25°) to the NNW. The thrusts have displaced Ediacaran dykes (Fig. 5d). Rocks in the south and southeast of the island are slightly deformed (Fig. 4a). They dip gently (up to 12°) to the WNW. Open small-scale folds (F_1^H) are rare. Volcaniclastic rocks in the east and north are weakly deformed too. Unit B is overlain by basalts of Late Cambrian age (Unit C) (491.2 ± 2.2 Ma, plagioclase, $^{40}Ar/^{39}Ar$, Prokopiev et al., 2017) (Fig. 4). Deformations of the second stage (D_2^H) are represented by F_2^H–folds with relatively steeply dipping axes (up to 60–70°) (Fig. 5f). These folds are associated with NW-SE-trending strike-slip faults with a reverse slip component. These faults deformed Late Cambrian basalts (Unit C) (Fig. 4a). Undeformed thin mafic dykes intruded Late Cambrian basalts. Ediacaran and Middle-Upper Cambrian volcaniclastic rocks contain basaltic trachyandesite sills (419.2 ± 3.7Ma, $^{40}Ar/^{39}Ar$) (Ershova et al., 2016a). Therefore, it is possible that the undeformed dykes are also of Late Silurian-Early Devonian age, and their formation coincided with the second deformation stage (D_2^H). There are small-scale normal faults with fault planes inclined to the east and west, which have displaced deformed rocks in the southern part of the island (D_3^H).

2.2.3. Structural studies of Bennett Island

Cambrian and Ordovician carbonate and clastic rocks are exposed on Bennett Island (Danukalova, 2016; Kos'ko et al., 1985) and are deformed into a broad anticline F_1^B with a width of up to 20 km (D_1^B) (Kos'ko et al., 1985). The limbs of this fold dip gently (10–15°) to the ENE and WSW (Fig. 6). The anticlinal axis plunges gently to the NNW. Cleavage is absent. Some small-scale N-S-trending reverse faults have been observed. The folded strata are overlain with an angular unconformity by Cretaceous basalts dated as 106–124 Ma (Drachev, 1999; Fedorov et al., 2005).

2.2.4. Low-temperature thermochronology ((U-Th)/He studies)

AHe and ZHe ages from the six samples collected from the De Long islands have been obtained (Fig. 7a, b). The AHe ages from the Cambrian rocks of Jeannette Island (sample13AP24) are Cenozoic in age, averaging at ca. 53 Ma. The 13AP26 ZHe ages from the same formation show a range of middle Paleozoic ages averaging at 414 ± 15 Ma.

The three samples from Henrietta Island exhibit a different exhumation-cooling history. AHe ages obtained from the sandstone (sample 13AP68, Unit B), collected in the less deformed southeastern part of the island, exhibit a wide dispersal of ages, suggesting that samples were located in the partial resetting zone for a long period of time. This suggestion has been supported by further modelling. The 13AP59 sample originated from the more intensely deformed southwestern part of the island and contains much younger mainly Cretaceous AHe ages. The ZHe ages from the 9-va-13-38 samples show a range of middle Paleozoic ages averaging at ca. 398 ± 22 Ma. The ZHe ages from the Lower Ordovician deposits of Bennett Island show ages between 470 and 318 Ma, averaging at 378 ± 38 Ma.

2.2.4.1. Thermal modelling of (U-Th)/He data. Inverse thermal history modelling was performed using 4 grains from sample 13AP68 (Fig. 8A) from the eastern, undeformed section of Henrietta Island. Model results indicate a protracted heating and cooling history throughout the Phanerozoic, residing at temperatures < 90 °C since the Carboniferous and cooling to surface temperatures from the Early Jurassic to present. Forward modelling tests the effects of increasing maximum burial temperature from 80 to 140 °C, and model results indicate that much of the AHe date dispersion can be replicated when a range of annealing kinetics are taken into account (Fig. 8B). Our models suggest that old

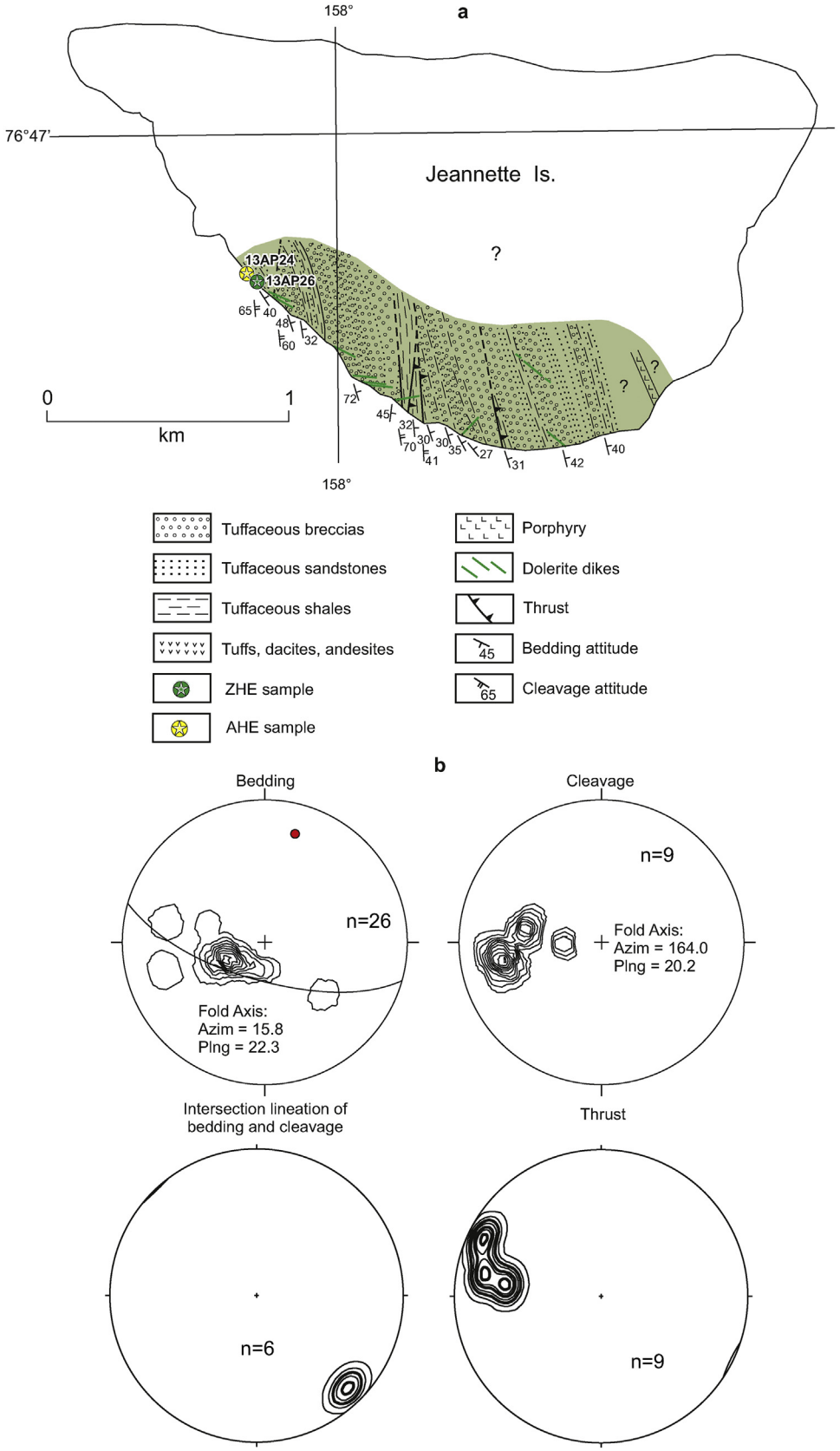

Fig. 2. (a) Simplified geological map of southern part of Jeannette Island, modified from Ershova et al. (2016a); (b) bedding, cleavage S_1^J, bedding-cleavage intersection lineation L_1^J and thrusts diagrams (equal-area projection, lower hemisphere; n – number of measurements). (For interpretation of the references to colour in this figure legend, the reader is referred to the web version of this article).

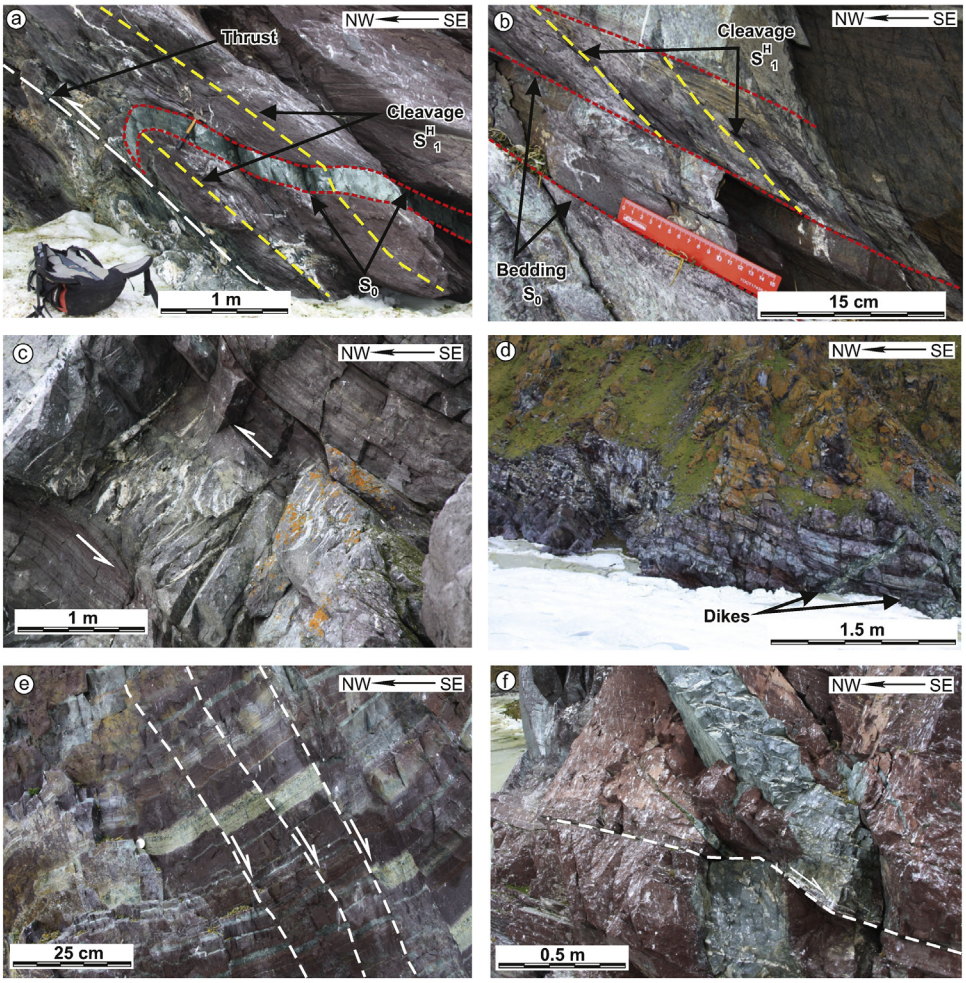

Fig. 3. Structures on Jeannette Island: (a) fold F_1^J accompanied by the axial plane cleavage S_1^J, dipping towards the east. zones; (d) mafic dykes; (e) normal faults with fault planes inclined to the east; (f) normal faults displace Ediacaran dyke. (For interpretation of the references to colour in this figure legend, the reader is referred to the web version of this article).

AHe dates with low eU concentrations may be meaningful data, as they can be explained by apatite with retentive annealing kinetics that have been accumulating radiation damage for substantial time periods prior to deposition. Whereas all modelled temperatures yield date-eU trends that can account for most of the AHe data, one possible interpretation is that 140 °C is perhaps too high a temperature, as some of the AHe dates do not fall within the AHe inheritance envelope. Forward models of ZHe data (Fig. 8C) indicate that progressively more ZHe data are accounted for as maximum temperatures increase from 80 to 140 °C. For these reasons, we suspect that maximum burial temperatures of Henrietta Island are likely in the range of 110–140 °C. Comparatively, modelling of sample 13AP59 from the western faulted region of Henrietta Island requires a discrete thermal history from 13AP68, experiencing a more protracted cooling history at higher temperatures from the Jurassic through Late Cretaceous (Fig. 8A).

The inverse model for Jeannette Island (Fig. 9A) only constrains the Cenozoic cooling history of the Island and provides limited information on maximum temperatures, due to the small range in eU concentrations and limited AHe date dispersion in sample 13AP24. As a result, forward models follow the same burial history as Henrietta Island (Fig. 8A). Inheritance envelopes for ZHe data indicate that temperatures between 110–140 °C are sufficient to account for most of the ZHe data in sample 13AP26 (Fig. 9C). Whereas the 140 °C forward model is within error of many of the dates from sample 13AP74 from Bennett Island, it is possible that Cambrian-Ordovician strata experienced higher temperatures.

2.3. Anjou Islands

2.3.1. Structural studies of Kotel'nyi Island

Kotel'nyi Island comprises a deformed Ordovician to Jurassic sedimentary succession unconformably overlain by Lower Cretaceous sandstones and volcanic deposits in the central part of the island, with a limited distribution of Cenozoic rocks filling in small grabens and depressions. The Paleozoic history of deformation on Kotel'nyi Island is poorly understood. An angular unconformity at the base of the Lower Carboniferous strata was identified in the southwest of Kotel'nyi Island, where Lower Carboniferous rocks lie on Ordovician, Silurian and Devonian strata, but has been poorly studied to date (Kos'ko et al., 1985).

Intrusive rocks include a small number of dykes, stocks, and sills of middle to late Paleozoic diabase and gabbro-diabase, typically 6–7 km long and up to several tens of meters thick. The dykes mainly have a NW-SE strike. Some late Mesozoic NW-SE striking dolerite dykes up to several tens of meters in thickness have intruded into Triassic rocks (Dorofeev et al., 1999; Kos'ko et al., 1985; Kos'ko and Korago, 2009; Prokopiev et al., 2017) (Fig. 10). Exposed tectonic structures in Kotel'nyi Is. form part of a fold-and-thrust belt. The NW striking Chokur anticlinorium, the Balyktakh synclinorium, and the Reshetnikov anticlinorium are recognized from south to north (Fig. 10).

The rocks of Kotel'nyi Island are deformed into north-west trending folds accompanied by NW-SE trending thrusts (Kos'ko et al., 1985; Kos'ko and Korago, 2009). One of the largest is the Mikhailov thrust,

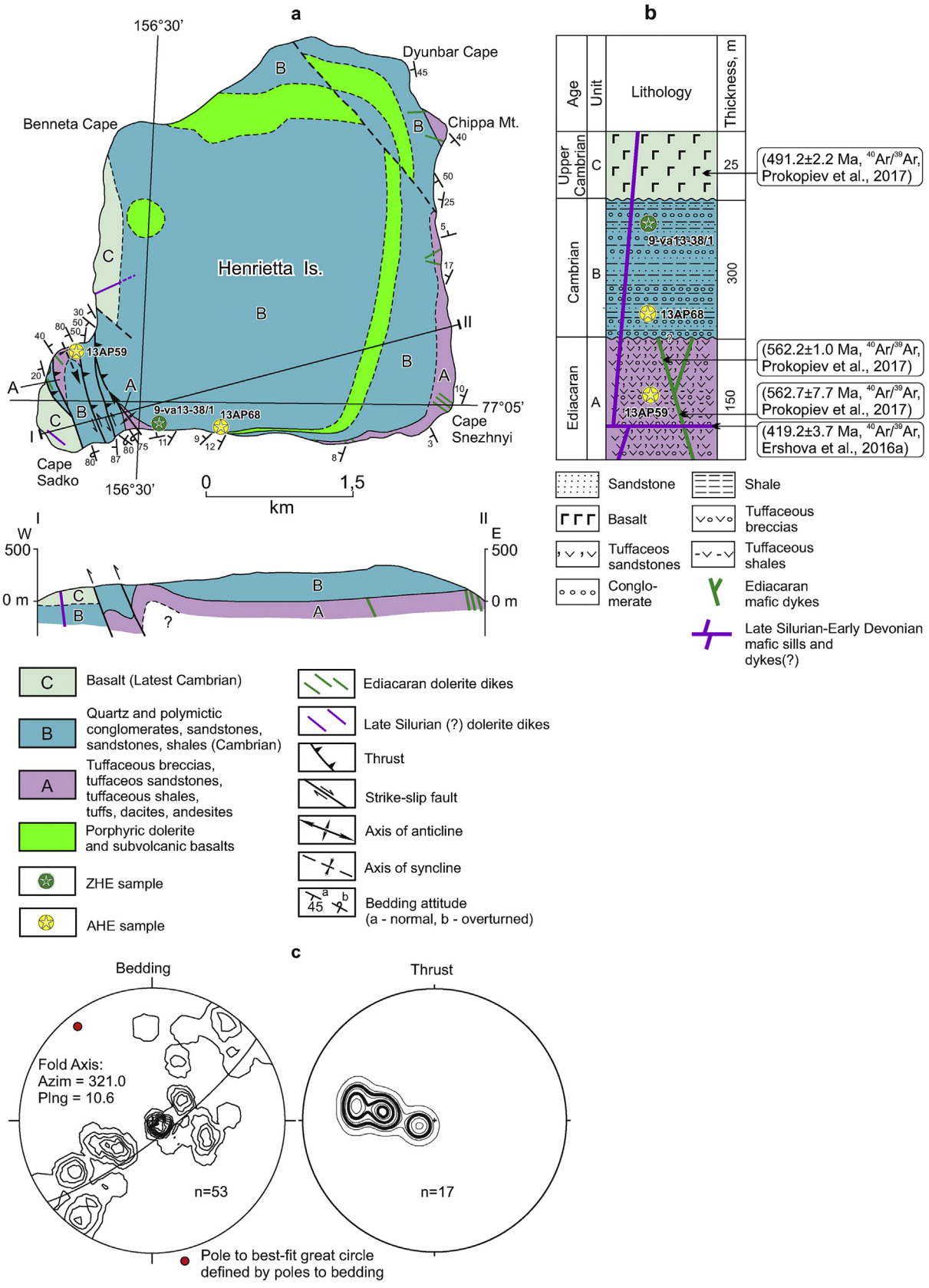

Fig. 4. (a) Simplified geological map of Henrietta Island, modified from Ershova et al. (2016a), Kos'ko and Korago (2009) and Vinogradov et al. (1975) and geological cross-section; (b) stratigraphic column, modified from Ershova et al. (2016a); (c) pole to bedding and thrust plane diagrams (equal-area projection, lower hemisphere; n – number of measurements). (For interpretation of the references to colour in this figure legend, the reader is referred to the web version of this article).

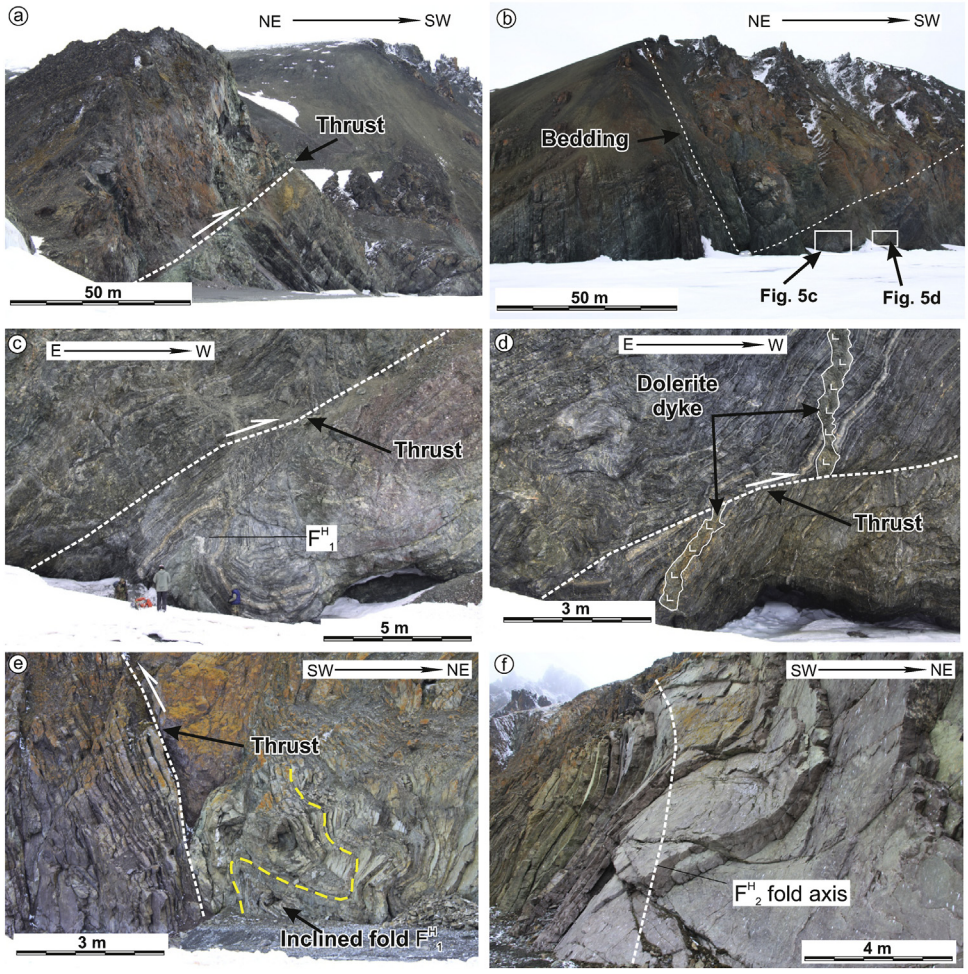

Fig. 5. Structures on Henrietta Island: (a) west-directed thrust (D^H_1); (b) NNW-SSE trending F^H_1 folds; (c) small-scale west-directed thrust (D^H_1); (d) the thrust have displaced Ediacaran dyke; (e) F^H_1–folds overturned to the WSW; (f) F^H_2–folds with relatively steeply dipping axes (D^H_2). (For interpretation of the references to colour in this figure legend, the reader is referred to the web version of this article).

separating the Balyktakh synclinorium and the Chokur anticlinorium. Within the Balyktakh synclinorium and the Reshetnikov anticlinorium, there are approximately N-S and NW-SE striking dextral strike-slip faults (Upper-Balyktakh, Tuor-Yurekh and Kozhevin faults) (Fig. 10) (Drachev, 1989; Kos'ko et al., 1985) with up to 10 km horizontal displacements, which have displaced Lower Cretaceous deposits. Structural relationships between the thrusts and strike-slip faults are unclear. S-shaped bending of fold axes associated with the thrusts indicate that they are older in age than the strike-slip faults (Kos'ko and Korago, 2009; Parfenov and Kuz'min, 2001).

According to Kos'ko and Korago (2009), two generations of fold and thrust structures are recognized – 1) NW-SE trending early thrusts probably with a strike-slip component and associated folds, and 2) N-S-trending normal and strike-slip faults.

Brandes et al. (2015) reported that in the central part of the island E-W and NNW-SSE trending fractures are developed. In the NW of the Island, N-S and NE-SW-trending fractures dominate. There is evidence for NNE–SSW-trending sinistral strike-slip faults. In the SW of the island, fracture sets dominate, consisting of NNE–SSW- and NW–SE-trending joints. In addition, NW–SE-oriented sinistral strike-slip faults occur.

According to previous studies, the deformation structures on Kotel'nyi Island were related to two main geodynamic events: 1) the closure of the South Anyui (Angayucham) Ocean basin and formation of the South Anyui suture (contractional structures) in Early Cretaceous time, and 2) the subsequent opening of the Eurasian Basin (extensional structures) in Late Cretaceous-Cenozoic times (Kos'ko and Korago, 2009; Nokleberg et al., 2001; Parfenov and Kuz'min, 2001; Brandes et al., 2015; Piepjohn et al., 2017 and references therein). The continuation of the South Anyui suture in the Laptev Sea shelf and in the area of the NSI is open to discussion. Some authors suppose it is located in the central part of the Anjou Islands (Fujita et al., 1997; Natal'in et al., 1999; Parfenov et al., 1993a, b; Spektor et al., 1981), others place it to the west of Kotel'nyi and Bel'kovsky Islands (e.g. Brandes et al., 2015; Drachev et al., 1998; Drachev, 2002; Franke et al., 2008), whilst others think that Kotel'nyi Island is a separate passive margin terrane (Drachev et al., 2010). It is also suggested that the South Anyui suture continues to the east of the De Long Islands (Metelkin et al., 2014, 2015). Piepjohn et al. (2017) suggested that the South Anyui Suture Zone is truncated by a N-S trending dextral fault zone, which was responsible for the NW-SE trending structures on Kotel'nyi and Belkovski islands, and which has later been reactivated by extension of the Laptev Sea Rift. Recent U-Pb detrital zircon studies of the Paleozoic succession of the NSI showed similar provenance fingerprints of Cambrian to Carboniferous deposits, indicating that the New Siberian Islands were part of the same tectonic plate and have experienced a similar geological evolution throughout the Paleozoic (Ershova et al., 2015a,b, 2016a,b; Ershova et al., 2018).

There are several geological constraints defining the sequence and age of deformation across the Anjou islands:

1 The main folding, shown on all geological maps, has a NW-SE trend

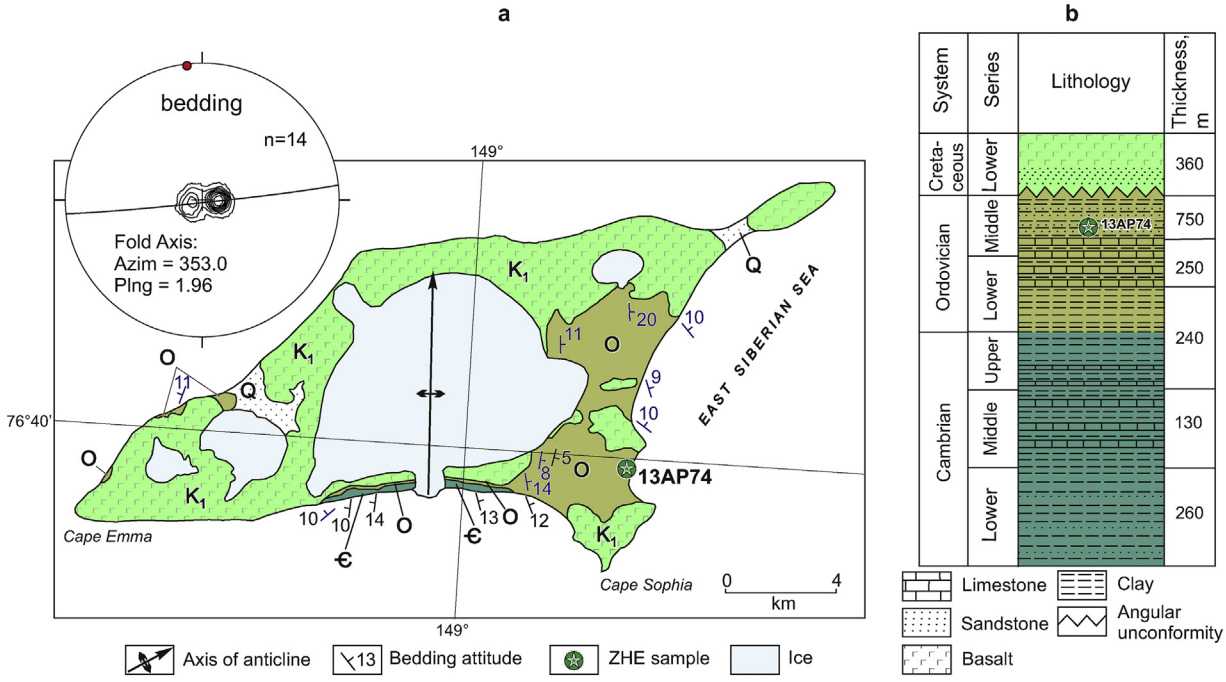

Fig. 6. (a) Simplified map of Bennett Island and bedding diagram (equal-area projection, lower hemisphere; n – number of measurements); (b) stratigraphic column, modified from Danukalova (2016), Ershova et al. (2016a) and Kos'ko and Korago (2009). ϵ – Cambrian, O – Ordovician, K_1 – Lower Cretaceous, Q – Quaternary. (For interpretation of the references to colour in this figure legend, the reader is referred to the web version of this article).

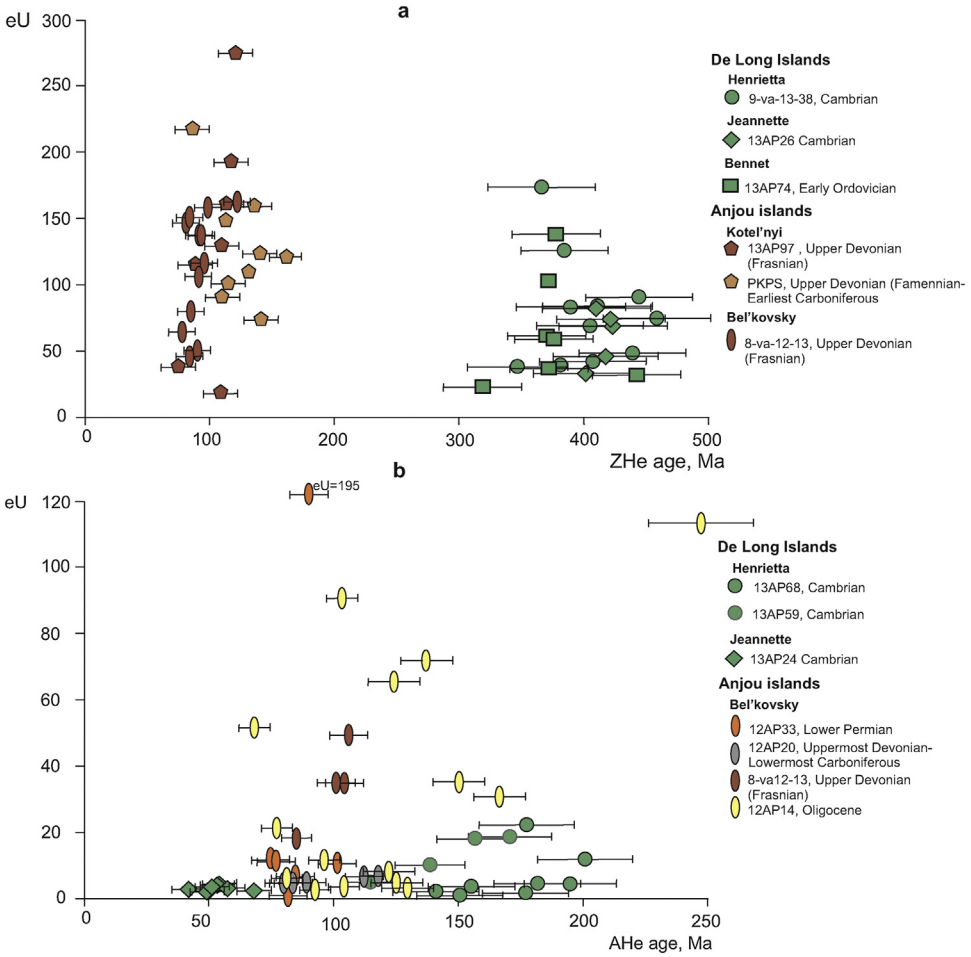

Fig. 7. (a) (U-Th)/He zircon ages plotted against e(U) concentration; (b) (U-Th)/He apatite ages plotted against e(U) concentration. See text for discussion. (For interpretation of the references to colour in this figure legend, the reader is referred to the web version of this article).

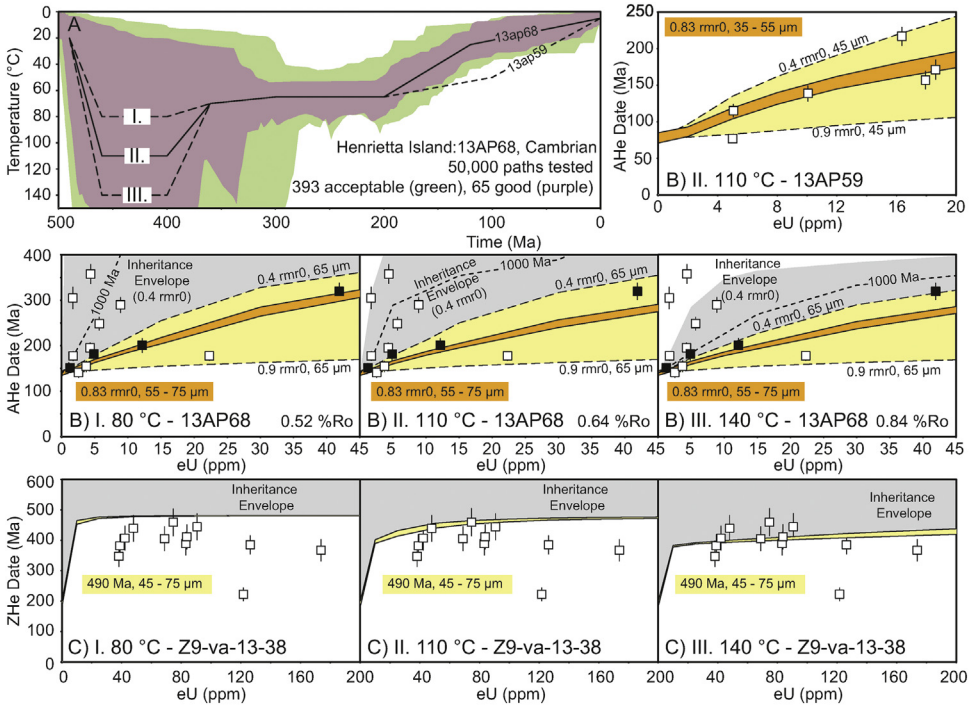

Fig. 8. Thermal history models for Henrietta Island. (A) Inverse thermal history model for sample 13AP68, as well as three t-T histories (I, II, III) invoked in forward modelling. Dashed line indicates the proposed cooling history for 13AP59. An inverse model for this sample is included in the online data repository. (B) AHe forward models for 13AP68 and 13AP59. Models show probable date-eU trends for a range of grain size and annealing kinetics (rmr0: Carlson et al., 1999; Ketcham et al., 2007). Apatite dates in black indicate data incorporated into the inverse thermal history model. (C) ZHe forward models that highlight the expected "inheritance envelope" (Guenthner et al., 2015) that encompasses modelled ZHe date-eU trends for all possible predepositional histories in the detrital zircon population. (For interpretation of the references to colour in this figure legend, the reader is referred to the web version of this article).

and affected Ordovician-Jurassic rocks across Kotel'nyi and Bel'kovsky islands, as well as to the east on the Zemlya Bunge Island (Kos'ko et al., 1985; Kos'ko, Korago, 2009; Trufanov et al., 1986).

2 An unconformity (possibly angular) truncated the Paleozoic, Triassic and Jurassic rocks at the base of the Aptian-Albian deposits in the central part of the island (Kos'ko et al., 1985; Kos'ko, Korago, 2009; Kuzmichev et al., 2009; Nepomiluev et al., 1979).

3 Aptian-Albian deposits of the central part of Kotel'nyi island are deformed into a wide asymmetric (dip reaches 45–60° on eastern limbs and 5–8° on the western) low-amplitude syncline with a N-S and NNW-SSE trend of the axial trace (Kos'ko et al., 1985; Kos'ko and Korago, 2009; Kuzmichev et al., 2009). The strike of Aptian-Albian deposits sharply differs from the NW-SE trend of the underlying folded strata. These structures cannot be the result of glaciotectonics during regional glaciation in the second half of the middle Pleistocene, as deformation described from the Novaya Sibir Island (Danukalova and Kuzmichev, 2014; Piepjohn et al., 2017) the glacier did not reach the central part of the Kotel'nyi Island or Bel'kovsky Island (Basilyan et al., 2009, 2010).

4 Large dextral strike-slip faults in the central part of Kotel'nyi Island

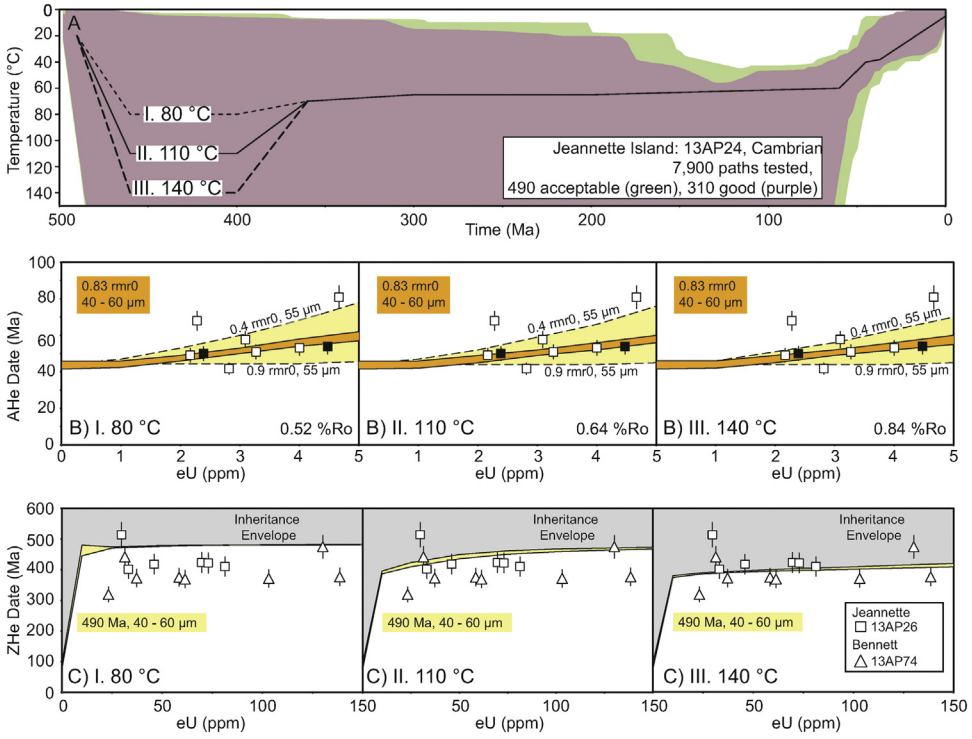

Fig. 9. Thermal history models for data from Jeannette and Bennett islands. (A) Inverse thermal history model for sample 13AP24, as well as three t-T histories (I, II, III) invoked in forward modelling. (B) AHe forward models for 13AP24. Models show probable date-eU trends for a range of grain size and annealing kinetics (rmr0: Carlson et al., 1999; Ketcham et al., 2007). Apatite dates in black indicate data incorporated into the inverse thermal history model. (C) ZHe forward models that highlight the expected "inheritance envelope" (Guenthner et al., 2015) that encompasses modelled ZHe date-eU trends for all possible predepositional histories in the detrital zircon population. ZHe data are plotted for both Jeannette and Bennett islands. (For interpretation of the references to colour in this figure legend, the reader is referred to the web version of this article).

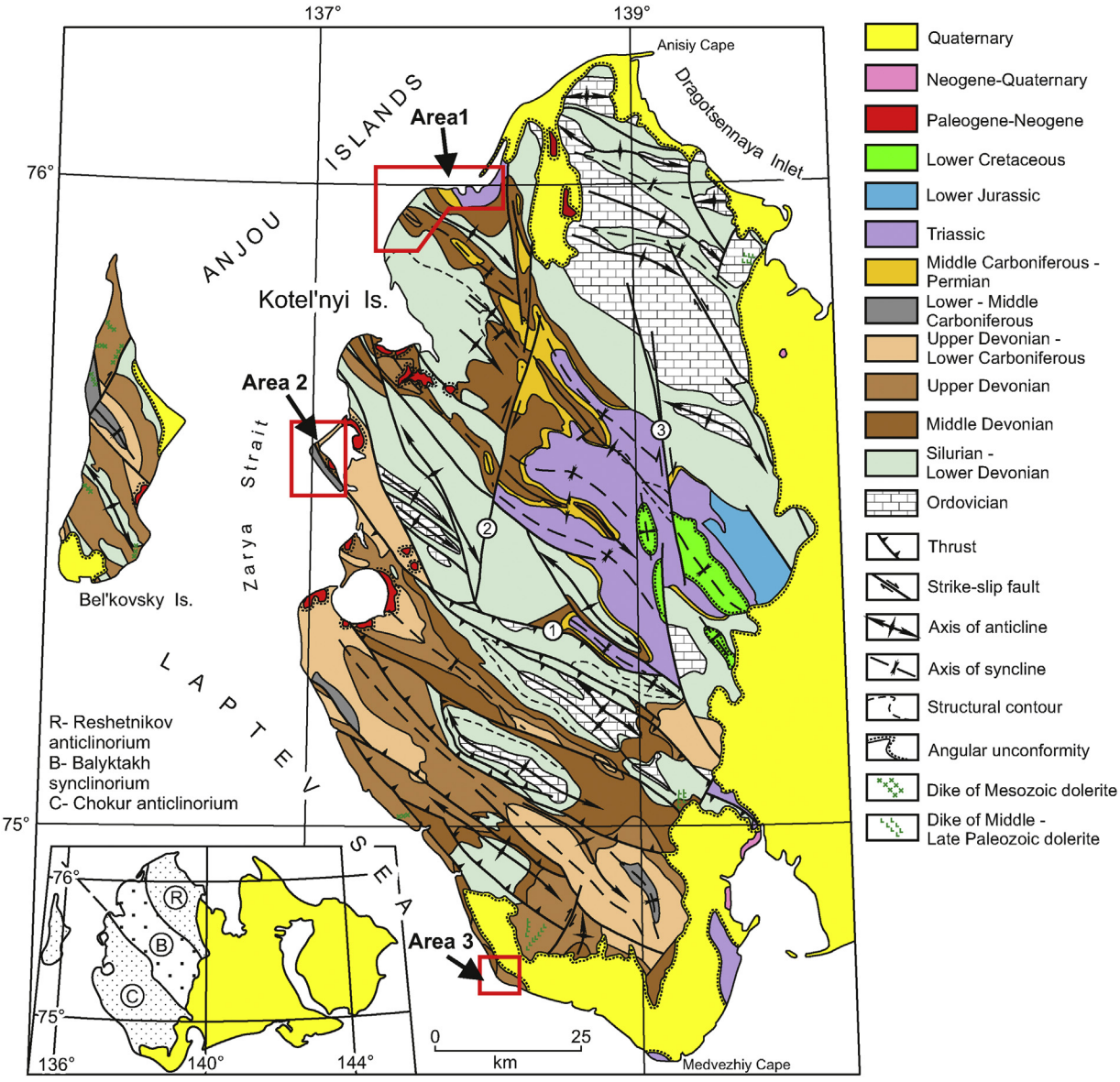

Fig. 10. Geological map of the Belkovsky Island and western Kotel'nyi Island with location of study areas (red rectangulars). Shown in the lower left corner is a tectonic zonation sketch map (modified from Parfenov and Kuz'min, 2001). Faults: 1 – Mikhailov thrust, 2 – Upper-Balyktakh dextral strike-slip, 3 – Tuor-Yurekh dextral strike-slip fault. R – Reshetnikov anticlinorium, B – Balyktakh synclinorium, C – Chokur anticlinorium. (For interpretation of the references to colour in this figure legend, the reader is referred to the web version of this article.)

predominantly have N-S strike and displace both the folds with NW-SE strike and the Aptian-Albian sediments (Kos'ko et al., 1985; Kos'ko and Korago, 2009).

5 The limited distribution of Paleogene-Neogene deposits overlie older folded rocks with a sharp angular unconformity and often fill in small grabens.

2.3.1.1. Station Lagoon (Area 1). Area 1 comprises Devonian and Carboniferous (?) deformed carbonate rocks and Permian –Triassic clastics overlain by subhorizontal Neogene-Quaternary deposits (Figs. 10 and 11). In general, the Devonian – Triassic rocks are deformed into NW-SE-striking concentric and cylindrical folds of varying size, which are associated with SW- and NE-dipping thrusts. According to detailed structural studies, the following several stages of deformation are recognized here.

The deformations of the first stage (D_1^K) are represented by folds and thrusts of WNW-ESE strike, involving Lower Devonian strata of the Basykh-Karga Formation (locality 11) and Shlyupka Formation (locality 37), along with Middle Devonian rocks of the Sokolov Formation in the north and west of Area 1 (locality 3 and 40, respectively) (Fig. 12).

The deformed Middle Devonian rocks are unconformably overlain by Upper Devonian rocks. The angular unconformity is exposed in locality 40, ~1.5 km southwest of the Sokolov River mouth. Here, the deformed Middle Devonian carbonates of the Sokolov Fm. are overlain by alternating varicolored clays and siltstones with subordinate beds of marls, bioclastic limestones and sandstones of the Upper Devonian (Frasnian) Nerpalakh Fm. (Fig. 12). The Middle Devonian rocks are dipping to the NNE and are affected by S-SW-vergent folds F_1^K and by thrust faults of the same transport direction (Fig. 13a; diagrams 9, 10 in Fig. 12). Cleavage is absent. The fold axes plunge gently (< 11–21°) to the ENE (51–80°) (diagrams 9, 10 in Fig. 12), almost orthogonal to the general NW-SE strike of folding on Kotel'nyi Island. The overlying Upper Devonian rocks are located on the south-west limb of an open fold with a width of ~600 m and a dip of 35° to the NE. The axis of this superimposed fold is inclined to the NW (az. 308°) at an angle of 30° (diagram 14 in Fig. 12), parallel to the axes of major fold structures on

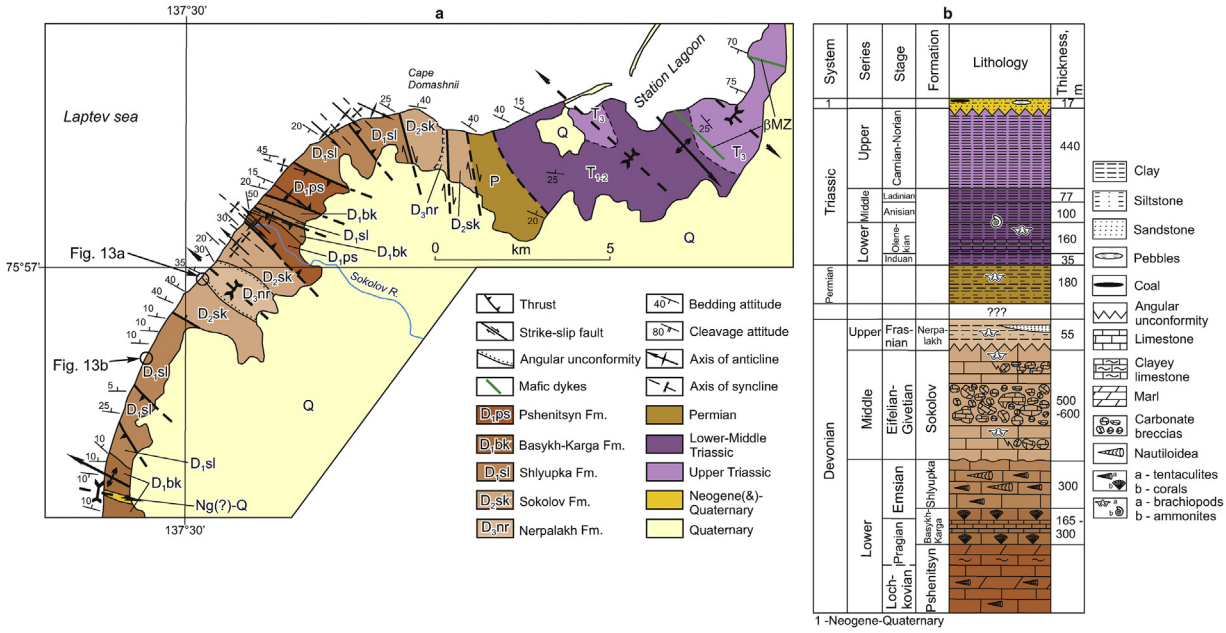

Fig. 11. Geological map of Area 1 (a) and stratigraphic column (b) (modified from Prokopiev et al., 2018; Kos'ko et al., 1985). For location see Fig. 10. (For interpretation of the references to colour in this figure legend, the reader is referred to the web version of this article).

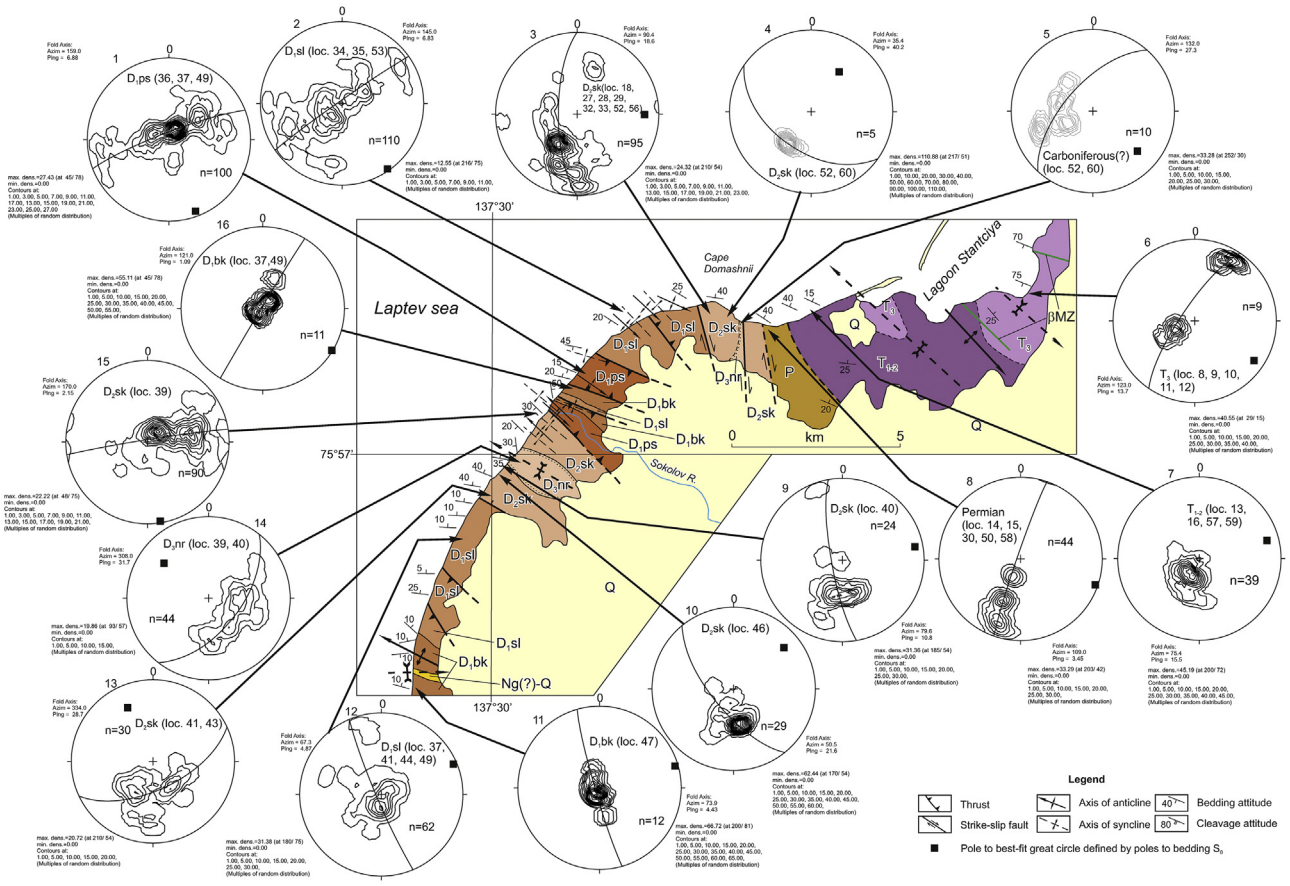

Fig. 12. Geological map of Area 1 (modified from Kos'ko et al., 1985) with pole-to-bedding diagrams (equal-area projection, lower hemisphere; n – number of measurements). (For interpretation of the references to colour in this figure legend, the reader is referred to the web version of this article).

the island.

A few kilometers to the south from this exposure at locality 37, limestones of the Shlyupka Formation (Emsian) are deformed into tight to isoclinal folds F_1^K, striking W-E and cut by S-SW-directed thrusts (Figs. 12 and 13b). The Shlyupka Formation displays similar structural patterns to those observed in the Givetian limestones of the Sokolov Formation near the Sokolov River mouth. These similarities in structural style provide additional evidence that pre-Frasnian strata have a

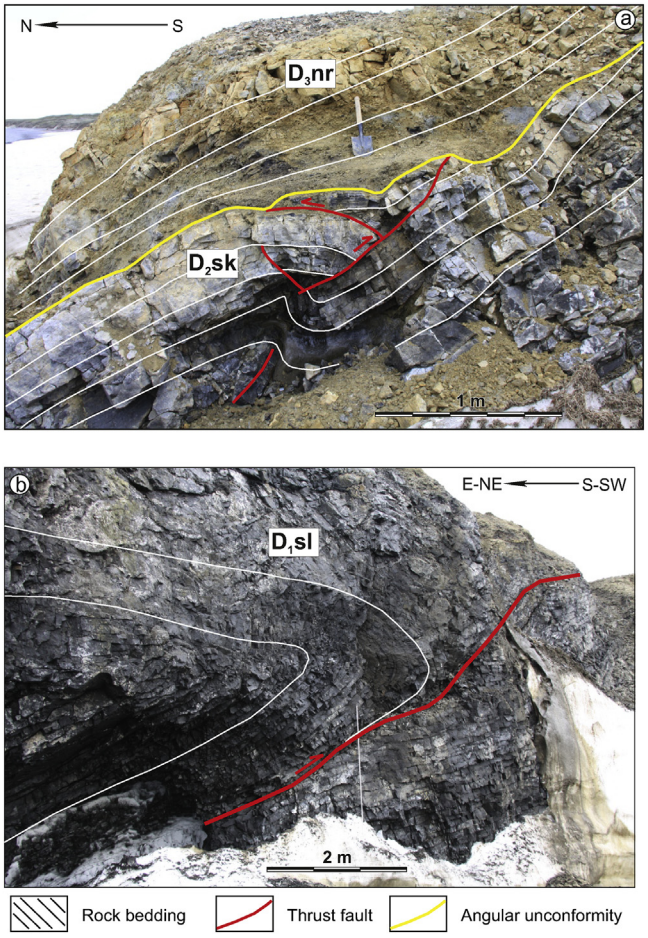

Fig. 13. An angular unconformity (yellow line) at the top of Sokolov Fm. (D_2sk) (Middle Devonian) overlain by Frasnian Nerpalakh Fm. (D_3nr) (Upper Devonian) (a) and tight to isoclinal fold overturned to NNE in Lower Devonian carbonates (Shlyupka Formation) modified from Prokopiev et al., 2018). (For interpretation of the references to colour in this figure legend, the reader is referred to the web version of this article.)

different structural style compared to overlying Paleozoic and Mesozoic succession across the study area, and were therefore involved in an older tectonic event which the younger Paleozoic and Mesozoic formations above the inferred unconformity did not experience. Thus, our studies show that the Lower-Middle Devonian rocks were folded before the Frasnian strata were deposited and that this event is determined as the first deformation stage (D_1^K).

The pre-Fransian angular unconformity is described from localities 52 and 60 (Cape Domashnii) (Fig. 12), where rocks of the Nerpalakh Formation also lie with angular unconformity on Sokolov Formation strata (Prokopiev et al., 2018).

The second deformation stage (D_2^K) structures are represented by major fold structures of Kotel'nyi Island, with a NW-SE trend easily observed in the Paleozoic and Mesozoic deposits across the island (diagrams 14, 5, 8, 6 and 7 in Fig. 12, respectively). The NW-SE trend is also observed in the underlying Lower-Middle Devonian rocks, which seem to have undergone D_1^K deformation. Diagrams 1, 2, 13, 14, 15 and 16 (Fig. 12) illustrate changes in the strike of measured and estimated axes of F_2^K folds of these rocks – from NW–SE to NNW – SSE (az. 121–159°) and their dip angles (1–30°).

The Permian clastic rocks dip to the northeast at 45–85°. They form an open syncline F_2^K of NW-SE strike (az. 109°, angle 4°) (Fig. 12).

The Triassic rocks over most of the study area dip to the northeast at 5–45°. In the NE, they are more steeply dipping (75–85°). We suppose that the rocks are deformed into two large asymmetric NW-SE striking F_2^K-synclines and an anticline in between them, overturned to the northeast. The width of these folds attains a few kilometers. Rocks of Upper Triassic age are exposed in the core of the synclines, while in its limbs and in the core of the anticline, exposures of Lower-Middle Triassic deposits are documented (Fig. 12). In the southwestern limb of the southwestern syncline, low-amplitude low-angle thrusts with SW-transport directions are developed (Fig. 14a).

The observed thrusts and associated small-scale folds of the second stage (D_2^K) dip mainly to the NE and SW (Figs. 14b and 15). Dip angles of the thrusts range widely, with angles of 60–90° predominating. Bedding-plane parallel detachment faults are widespread (Fig. 15) and slickenside lineations are almost perpendicular to the axes of F_2^K folds. The observed and estimated amount of displacement on the thrusts rarely exceeds a few tens of meters. The orientation of the thrusts and bedding-plane parallel detachment faults indicates that their formation is related to folding F_2^K.

Stress fields are restored based on slickenside lineations on thrusts and bedding-plane fault surfaces, suggesting a sub-vertical tension (σ_1) axis and sub-horizontal (NE-SW) compression (σ_3) axis, typical for environments characterized by regional compressive stresses. The intermediate (σ_2) axis is almost parallel to the NW-SE Kotel'nyi Island structural trend. Compression axis σ_3 gently plunges to the NE and SW, and is almost normal to F_2^K folds trend (Fig. 15).

Based on slickenside lineations and displacements of marker beds, sinistral and dextral strike-slip faults with a reverse component of displacement have been identified in the studied Paleozoic and Mesozoic succession (Figs. 14c and 15). These transfer faults were formed during the second stage of D_2^K deformation. Trends of sinistral strike-slip faults with a component of reverse displacement are mainly ENE-WSW, and dextral strike-slip faults are NNE-SSW (Fig. 15). According to our estimate, the amount of horizontal displacement along the transfer strike-slip faults ranges up to a few tens of meters. This was established by tracking the displacement of the marker bed along the outcrops of streams oriented sub-parallel to the strike-slip faults.

There are many ~ N-S trending thrusts (Fig. 15) of unknown origin. It can be assumed that there was a stage of W-E shortening during D_3^K, which led to deformation of the Aptian-Albian deposits of the central part of Kotel'nyi Island into asymmetric low-amplitude synclines with N-S and NNW-SSE trends (Kos'ko et al., 1985; Kos'ko and Korago, 2009; Kuzmichev et al., 2009).

N-S trending dextral strike-slip faults, dextral strike-slip faults with a reverse slip component and, possibly, dextral strike-slip faults with a normal slip component are associated with the fourth deformation stage (D_K^4). This component of normal slip does not contradict the structure of the strike-slip zones, since displacements can be associated with local extension. Sometimes these strike-slip faults are associated with steeply plunging small-scale folds. These faults are subparallel to N–S trending large dextral strike-slip faults in the central part of Kotel'nyi Island, which displaced both the folds of NW-SE strike and the Aptian – Albian deposits (e.g. Kos'ko et al., 1985; Kos'ko and Korago, 2009). Stress fields related to dextral strike-slip faults with horizontal striae on slickensides suggest that sub-horizontal tension and compression axes plunge to the SE and NE, respectively. The intermediate axis is vertical (Fig. 15).

In general, the stress field responsible for forming all thrusts, bedding plane faults and strike-slip faults was characterized by NE-SW compression, which was prevalent in the D_2^K-D_4^K stages.

Normal faults of the fifth stage (D_5^K) are common and characterized by a NNW-SSE trend (Figs. 14d and 15), deforming rocks both of Paleozoic and Triassic age. They dip steeply at 50–90°. The stress field related to normal faults is characterized by a horizontal tension (σ_1) axis, which gently plunges to the SW, and a compression (σ_3) axis which is sub-vertical. The intermediate (σ_2) axis is sub-horizontal and sub-parallel to the normal faults trend (Fig. 15). Thus, extension occurred in a WSW-ENE direction across Area 1. We can assume that sinistral strike-slip faults with a normal slip component of WNW-ESE and ENE-WSW

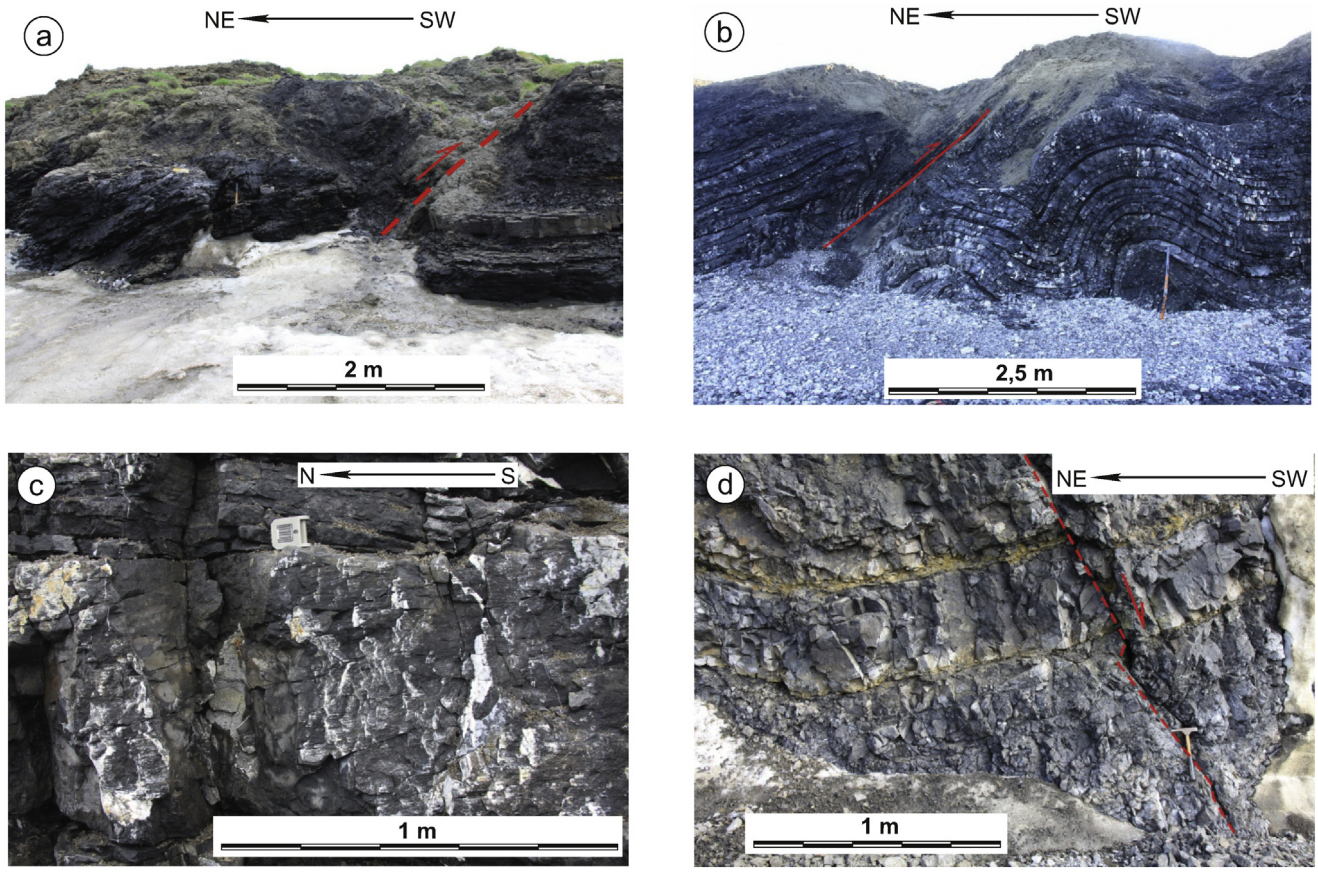

Fig. 14. Selected photo showing structures observed across Area 1: (a) SW-directed thrust fault in Lower Triassic rocks; (b) folded and thrust-faulted rocks of the Lower Devonian Shlyupka Formation. Transport along the thrust is towards SW; (c) dextral slickensides on the surface of NNE-SSW trending strike-slip fault; (d) normal fault in the Middle Devonian rocks with downthrow towards the WSW. (For interpretation of the references to colour in this figure legend, the reader is referred to the web version of this article.)

trends, and dextral strike-slip faults with a normal slip component of WNW-ESE trends, form transfer faults related to these normal faults. The tension (σ_1) axis for sinistral and dextral strike-slip faults with a normal fault component gently plunges to N–NW (Fig. 15).

2.3.1.2. Tas-Ary Island (Area 2). Tas-Ary Island itself represents the NE limb and core of the large Tas-Ary syncline, with a minimum width of 3–5 km. The core of the fold comprises deformed Frasnian-Lower Permian rocks. These folded rocks are overlain with a sharp angular unconformity by mildly deformed Paleogene-Neogene deposits (Fig. 16).

The Tas-Ary syncline has a NW-SE strike parallel to the main folding of the F_2^K stage on Kotel'nyi Island. Its axis dips gently towards the southeast (Fig. 16). This is also outlined by the orientation of the cleavage and bedding intersection lineation L_2^K (Figs. 16 and 17a). Bedding planes dip mainly to the southwest and northeast at 30–60°. The Tas-Ary syncline is NE-vergent, with steeply NE-dipping bedding-planes on the northeastern limb (up to 70°) and gently SW-dipping bedding-planes on the SW limb. In the limbs of the syncline, there are symmetric and asymmetric, concentric and cylindrical folds (F_2^K), with a width and amplitude ranging from a few meters to tens of meters (Fig. 18a, b). Orientation of their axes is close to the strike of the Tas-Ary syncline (Fig. 16). The mean fold axis of the Tas-Ary syncline plunges at 13° to the SE (dip az. 137°) (Fig. 16).

Cleavage S_2^K (Fig. 17b) occurs everywhere within Devonian-Carboniferous clastic rocks but is limited within massive carbonate units. There are observed cases of cleavage refraction (Fig. 17c). No cleavage is observed in the youngest Lower Permian succession in the northeastern limb of the Tas-Ary syncline and in its core. In general, the cleavage is fanning and has NW-SE strike and dips to the NE in the SW limb, and to the SW in the NE limb of the Tas-Ary syncline (Fig. 16). The NW-SE strike of folding and cleavage observed within Upper Devonian-Permian rocks in this area are similar to those which occur above the angular unconformity across Area 1. Consequently, we attribute these deformations to the second generation (D_2^K).

The observed thrusts and associated small-scale folds (F_2^K) plunge mainly to the NE and SW (Figs. 16 and 18c, d). Bedding-plane parallel detachment faults and contraction faults are widespread (Fig. 19). In general, the thrusts form imbricate fans with a wide range of dip angles, with angles of 50–70° predominating. The observed and estimated amount of displacement along the thrust faults is usually less than a few tens of meters.

Numerous strike-slip faults with a reverse or normal slip component cross-cutting the Tas-Ary syncline are observed (Figs. 16 and 17d), with locally associated small-scale folds with steep axes. Based on our measurements of the amount of displacement of the marker beds in outcrops of streams that are oriented orthogonally to the axis of the Tas-Ary syncline, we estimated the amount of horizontal displacement along the strike-slip faults to range up to a maximum of a few hundred meters. Trends of sinistral strike-slip faults with a reverse slip component are mainly WNW-ESE and NE-SW, and with normal slip component ENE-WSW, or more rarely NE-SW (Fig. 19). Trends of dextral strike-slip faults with a reverse slip component are mainly NNW-SSE and NNE-SSW, and with normal slip component ENE-WSW. These transfer faults were formed at the same stage of D_2^K as the Tas-Ary syncline, small folds of F_2^K, and thrusts of NW-SE strike.

Stress field restoration is based on shear fractures with reverse, strike-slip and normal fault displacement (Fig. 19). The stress field

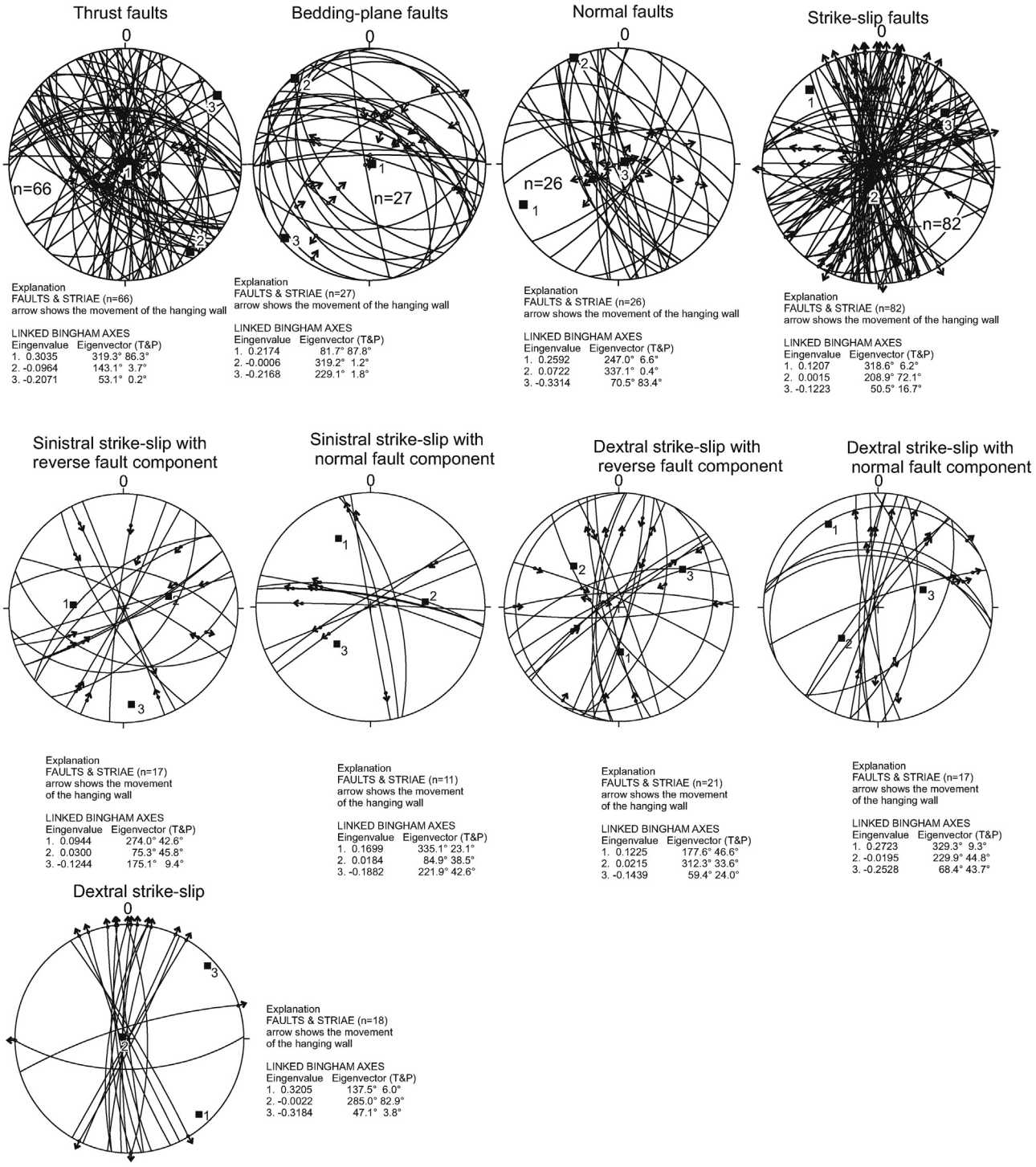

Fig. 15. Faults & striae data diagrams of Area 1. Axes: 1 – tension, 2 – intermediate, 3 – compression.

related to thrusts and bedding-plane faults is characterized by a sub-vertical tension (σ_1) axis and sub-horizontal compression (σ_3) axis, typical for regional compressive stress environments of the second deformation stage (D_2^K). The compression axis σ_3 gently plunges to the SW and is almost normal to the Tas-Ary syncline axis.

The stress field recorded by all transfer strike-slip faults is characterized by sub-horizontal tension (σ_1) and compression (σ_3) axes. The compression axis σ_3 gently plunges to the SW, and the tension (σ_1) axis to the SE. The intermediate (σ_2) axis is sub-vertical (Fig. 19). The tension axes estimated separately for the transfer sinistral and dextral strike slips with a reverse slip component are similar to those of the thrusts and bedding-plane faults, which indicates their formation in a single stress field together with the development of tectonic structures of the second stage (D_2^K) (Fig. 19).

There are several thrusts with a ~N-S trend of the third stage of D_3^K, which are widely manifested in Area 1 (Fig. 19).

Deformations of the fourth stage (D_4^K) are represented by the NNW-SSE and NNE-SSW trending dextral strike-slip faults (Fig. 19), which locally deform the cleavage of S_2^K. The stress field related to dextral strike-slip faults of NNW-SSE and NNE-SSW trends is characterized by a sub-vertical tension (σ_1) axis and a compression (σ_3) axis which plunges to the NE. (Fig. 19).

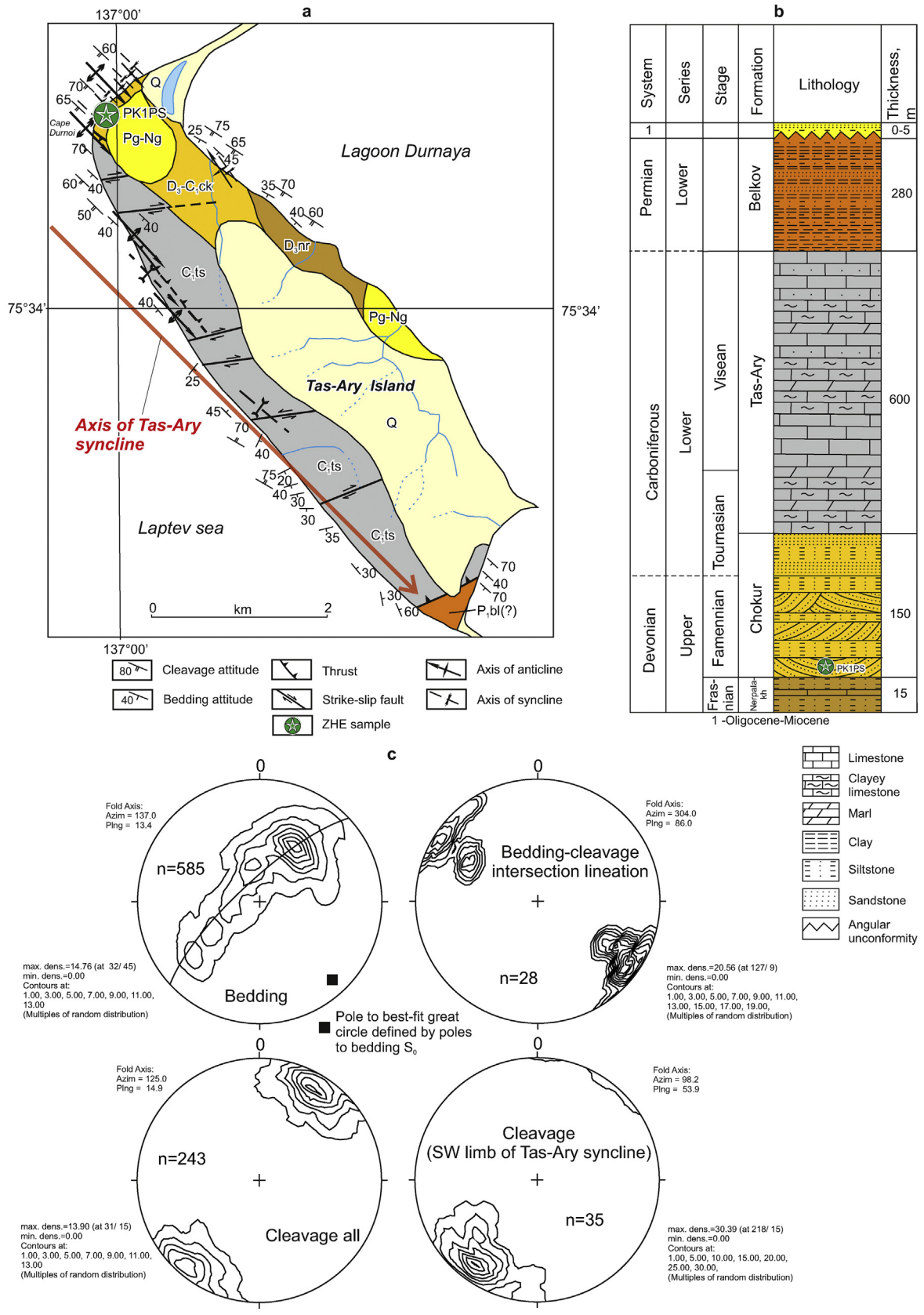

Fig. 16. (a) Geological map of Area 2; (b) stratigraphic column, modified from Kos'ko et al. (1985); (c) pole to bedding and cleavage, and intersection lineation diagrams (equal-area projection, lower hemisphere; n – number of measurements). Formations: D_3nr – Nerpalakh, D_3-C_1ck – Chokur, C_1ts – Tas-Ary, P_1bl – Bel'kov, Pg-Ng – Paleogene-Neogene, Q – Quaternary. For location see Fig. 10. (For interpretation of the references to colour in this figure legend, the reader is referred to the web version of this article.)

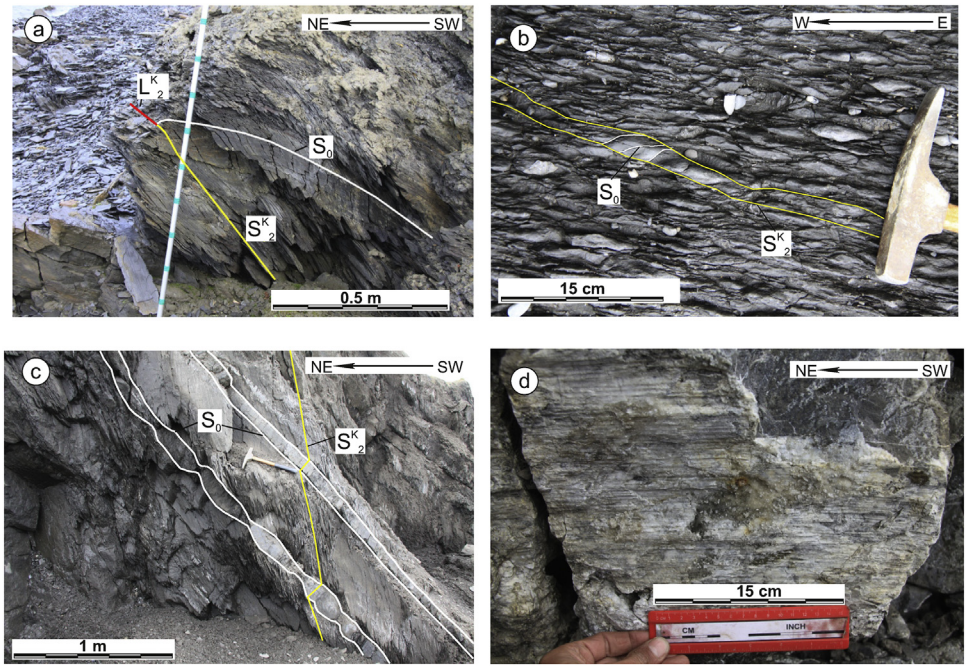

Fig. 17. Structures in Area 2: (a) the cross-cutting relationship of bedding and cleavage S_2^K in siltstones of the Nerpalakh Fm.; (b) relationships between bedding and cleavage S_2^K; (c) refraction of cleavage; (d) slickensides on the surface of transfer sinistral strike-slip fault of NE-SW trend. (For interpretation of the references to colour in this figure legend, the reader is referred to the web version of this article.)

In general, the stress field responsible for forming all thrusts, bedding plane faults and strike-slip faults is characterized by NE-SW-trending compression, which prevailed during the D_2^K–D_4^K stages.

The Cenozoic deposits are characterized by subhorizontal or slightly inclined bedding, and faulted by small-scale normal faults of the fifth stage (D_5^K) (Fig. 20a). The normal faults also deform the Paleozoic rocks (Fig. 20a, b). Dip angles of the normal faults are steep (70–90°). The faults mainly have a NE-SW trend (Fig. 19), which is different to the orientation of the normal faults in Area 1 (see Fig. 15).

The stress field related to the normal faults is characterized by a horizontal tension (σ_1) axis gently plunging to the SE, almost normal to the normal faults, and a sub-vertical compression (σ_3) axis. The intermediate (σ_2) axis is sub-horizontal (Fig. 19).

There is a single observation of the deformation of Paleogene-Neogene deposits by SW directed reverse faults (Fig. 20c), which can be attributed to the sixth deformation stage (D_6^K).

2.3.1.3. Anjou Cape (Area 3). Deformed terrigenous-carbonate rocks of Upper Devonian age (Nerpalakh Fm.) (Kos'ko et al., 1985) are exposed here in the core of a large F_2^K synclinal fold (Fig. 21), similar to Tas-Ary Island. The fold axis plunges to the WNW. Bedding dips to the WNW at 20–40° with superimposed cleavage of S_2^K (Fig. 21, diagram). Small folds are observed with axes oriented in the same direction as the axis of the large syncline F_2^K. The bedding-cleavage intersection lineation L_2^K also plunges to the WNW. Along the axial zone of the syncline, small WNW-trending thrust faults with a strike-slip component can be traced.

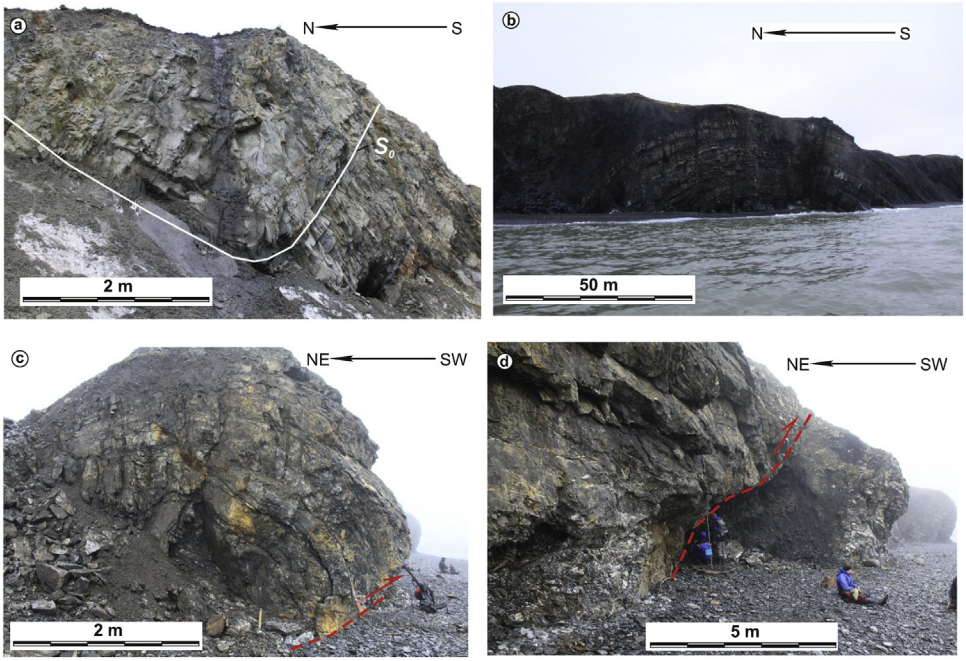

Fig. 18. Structures in Area 2: (a, b) Secondary fold-structures F_2^K in a tens- to hundreds-meters-scale on NE limb of the Tas-Ary syncline; (c, d) SW-directed thrust faults of D_2^K.

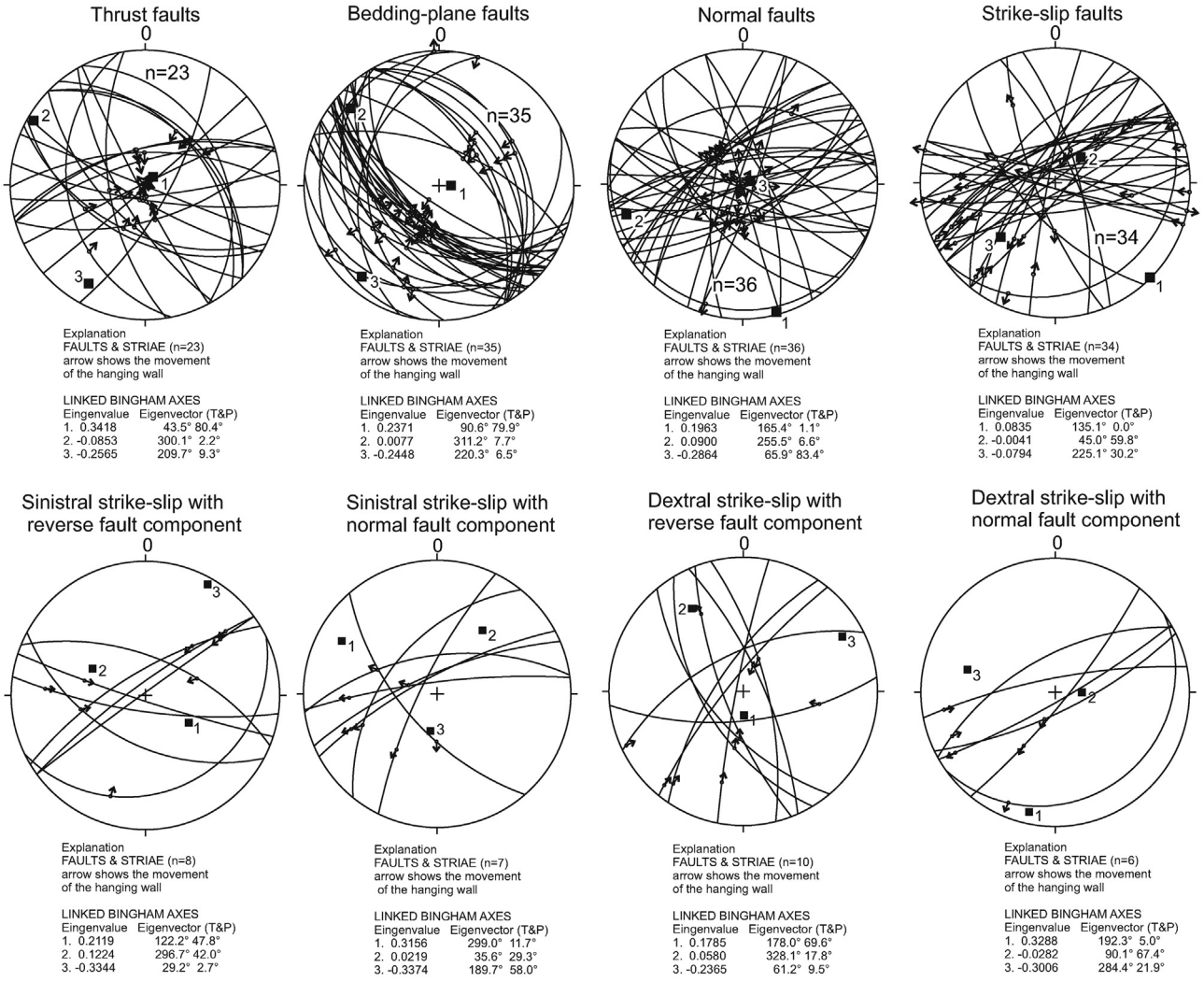

Fig. 19. Faults & striae data diagrams of Area 2. Axes: 1 – tension, 2 – intermediate, 3 – compression.

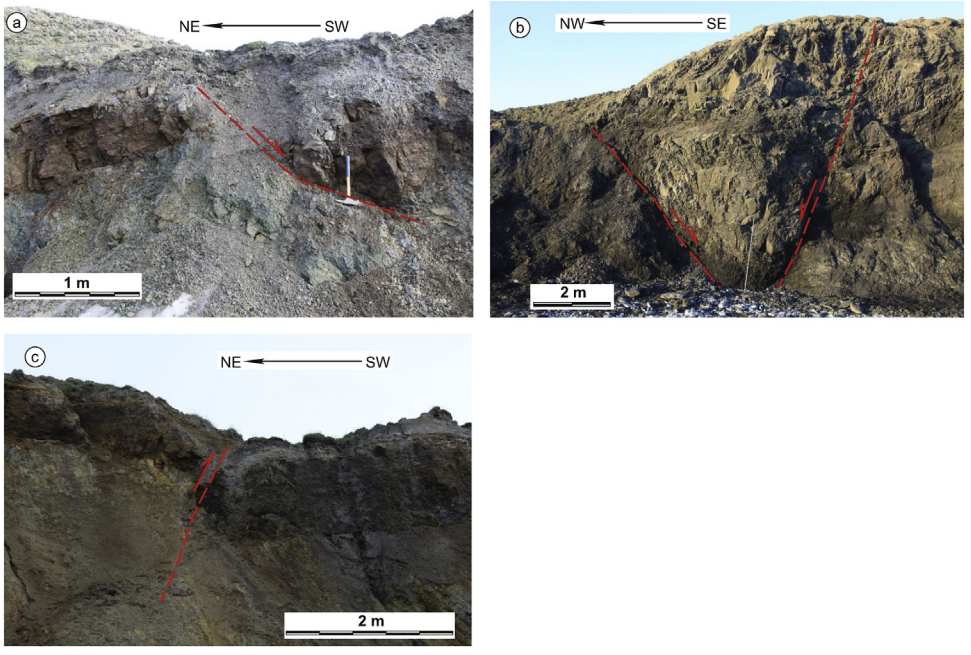

Fig. 20. Examples of faults postdating the main contractional deformation in the Area 2: (a) normal fault in the Paleogene-Neogene succession and sandstone of the Chokur Fm. (D_5^K); (b) normal faults-bounded small graben in the Paleozoic rocks (D_5^K). The faults mainly have a NE-SW trend; (c) SW directed reverse fault in the Paleogene-Neogene succession (D_6^K). (For interpretation of the references to colour in this figure legend, the reader is referred to the web version of this article.)

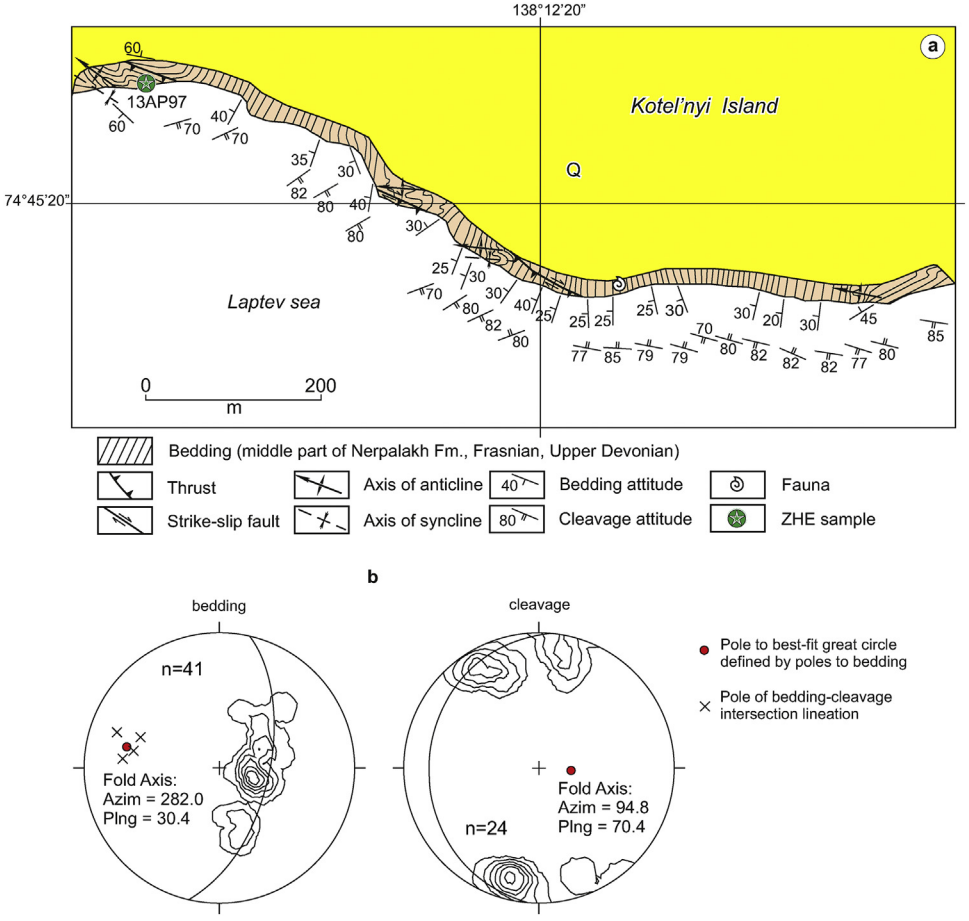

Fig. 21. (a) Simplified geological map of Area 3. For location see Fig. 10; (b) pole to bedding and cleavage diagrams (equal-area projection, lower hemisphere; n – number of measurements). (For interpretation of the references to colour in this figure legend, the reader is referred to the web version of this article.)

2.3.2. Structural studies of Bel'kovsky Island (southern part)

Bel'kovsky Island is located in the westernmost part of the NSI and comprises deformed Middle Devonian–Lower Permian mainly clastic successions, overlain with angular unconformity by Upper Eocene–Lower Miocene strata, filling in a small graben in the southeast of the island (Fig. 22a, b) (Brandes et al., 2015; Ershova et al., 2015b; Kos'ko et al., 1985; Kuzmichev et al., 2013; Piepjohn et al., 2017). The Paleozoic succession is intruded by Latest Permian and Middle Triassic mafic intrusions (Kuzmichev and Pease, 2007; Prokopiev et al., 2017).

The limited distribution of Middle Devonian rocks precludes direct observation of the pre-Frasnian angular unconformity across Bel'kovsky Island. However, Middle Devonian carbonates observed in the SE-part of the island are more intensely deformed than the overlying Upper Devonian to Permian strata. The Middle Devonian deposits of the Sokolov Formation are intensely brecciated and cut by chaotically oriented carbonate veins in the southeast of the island. The deformed Devonian-Permian rocks are mainly draped into wide open folds of NW-SE strike, similar to F_2^{Bl} of the second deformation stage (D_2^{Bl}) defined across Kotel'nyi Island (D_2^{K}). Rare small F_2^{Bl} folds striking NW-SE are open, asymmetrical, and cylindrical, with a width and amplitude up to a few meters (Fig. 23a). Discrete S_2^{Bl} cleavage of NW-SE strike dips to the SW in the southeast of Bel'kovsky Island, and to the NE in the southwest (Fig. 23b). Some intervals of the Nerpalakh Formation do not display any cleavage, which was also observed by Piepjohn et al. (2017). Dip angles of S_2^{Bl} cleavage range from subvertical to 30-50°. The general trend of cleavage and bedding intersection lineation L_2^{Bl} is NW-SE (Fig. 22c). Plunge of lineation locally ranges up to 50–60° (Fig. 23c). Reverse faults and thrusts, mainly with NE and SE transport directions, have dip angles ranging from 30–40° to 70–85° (Figs. 22c and 23 g). E-W-trending transfer strike-slip faults associate with thrusts (Fig. 23g). Their orientation is similar to that of the sinistral strike-slip faults described by Piepjohn et al. (2017) on Bel'kovsky Island. Small-scale shear zones characterized by both dextral and sinistral strike-slip kinematics are represented by en-echelon-arranged veins, deforming the Paleozoic sedimentary rocks and Permian-Triassic mafic intrusions. Rare bedding-plane parallel detachment faults have been described within the study area on Bel'kovsky Island.

The observed NNE-SSW-trending thrusts suggest the presence of third stage of deformation (D_3^{Bl}) (Figs. 22c and 23 g). The orientation of thrust planes and slickenside lineations suggests that the compression axis of D_3^{Bl} deformation is subhorizontal and has a WNW-SES strike (Fig. 23g).

Deformations of D_4^{Bl} are represented by dextral strike-slip faults of approximately N-S strike (Fig. 23d, g). Local minor deformation of S_2^{B}-cleavage, intersection lineation L_2^{B} and thrust planes is observed (Fig. 22c). The orientation of fault planes and slickenside lineations suggests that the compression axis of D_2^{Bl} and D_4^{Bl} deformation is subhorizontal and has a NE-SW strike, orthogonal to the trend of major folding in the region (Fig. 23g).

Normal faults of the fifth stage (D_5^{B}) have predominantly NW-SE to WNW-ESE strike and dip to the NNE, NE, SSW and SW, displacing Paleozoic rocks (Figs. 22c and 23 e, g). The amount of vertical displacement attains 0.5 m. Paleogene-Neogene rocks are also deformed by low-amplitude normal faults (displacement up to 20–30 cm), mainly of NW-SE strike and dipping towards the SW or NE (Fig. 23f). Two small-scale flexures are reported from Paleogene-Neogene deposits on the southeastern coast of the island. Their origin is unclear. On the one hand, they could represent an episode of late Cenozoic weak

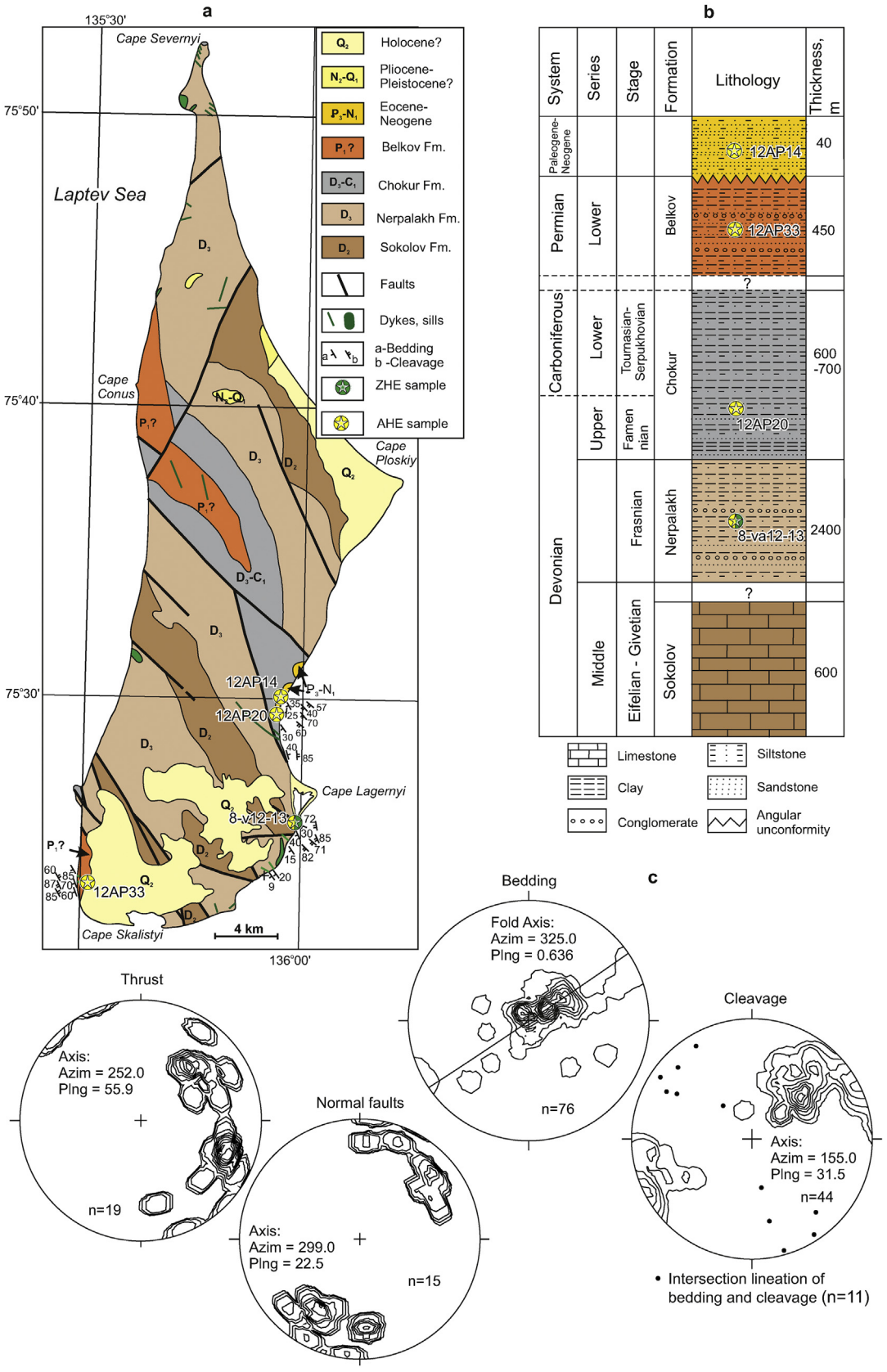

Fig. 22. (a) Simplified geological map of Bel'kovsky Island and (b) stratigraphic column (modified from Kos'ko et al., 1985). For location see Fig. 10. (c) pole to bedding S_0 and cleavage S_2^{Bl}, bedding–cleavage intersection lineation L_2^{Bl}, pole to thrust and normal faults diagrams (equal-area projection, lower hemisphere; n – number of measurements). (For interpretation of the references to colour in this figure legend, the reader is referred to the web version of this article.)

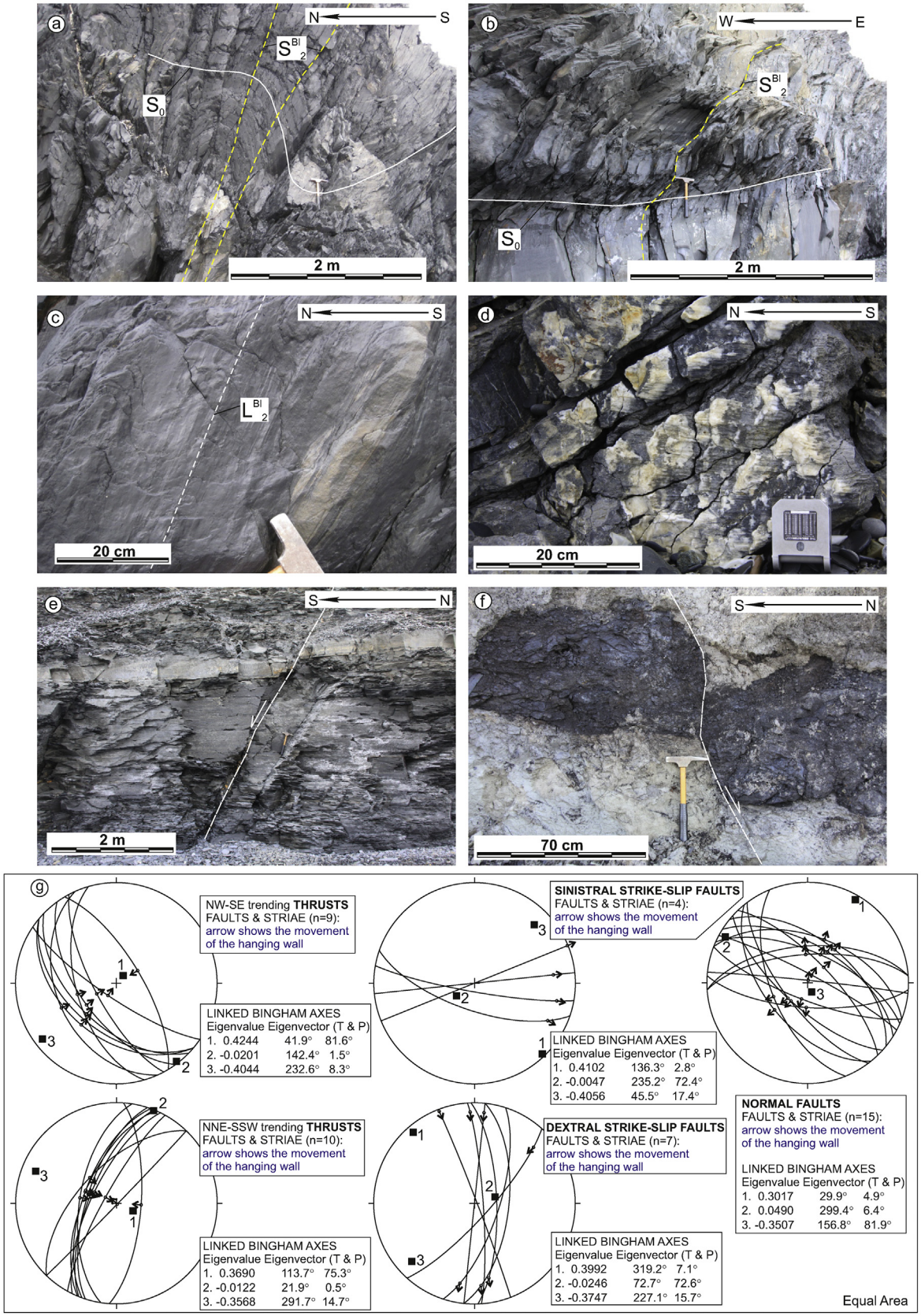

Fig. 23. Structures on Bel'kovsky Island: (a) small F_2^{Bl} folds striking NW-SE; (b) refraction of cleavage S_2^{Bl};(c) bedding-cleavage intersection lineation L_2^{Bl}; (d) slickenside lineations on the surface of a dextral N-S trending strike-slip fault (D_4^{Bl}); (e) normal fault in Nerpalakh Fm. of WNW-ESE strike (D_5^{B}); (e) normal fault in Eocene rocks of NW-SE strike (D_5^{B}); (g) faults & striae data diagrams. Axes: 1 – tension, 2 – intermediate, 3 – compression). (For interpretation of the references to colour in this figure legend, the reader is referred to the web version of this article.)

compression (D_6^B), but on the other hand, these flexures have been generated as propagation folds above buried normal faults.

The established sequence of deformation in this part of the island is, in general, consistent with the sequence determined across the western part of the island by earlier studies (Verzhbitsky, 2004, 2009).

2.3.3. Low-temperature thermochronology

2.3.3.1. (U-Th)/He studies. (U–Th)/He thermochronologic ages of detrital zircons and apatites have been collected from Devonian-Eocene strata of the Anjou Islands. All ZHe ages (13AP97, PK1-PS) obtained from the Upper-Devonian – Lower Carboniferous strata of Kotel'nyi Island are younger than the depositional age, suggesting a post-depositional resetting of the ages. Nine of eleven (U-Th/He) ages of detrital zircons from 13AP97 displayed Late Cretaceous ages, averaging at ca. 106 Ma. Sample PK1-PS exhibited a broad range of ZHe ages, averaging around 125 Ma. Sixteen ZHe ages obtained from the Upper Devonian sandstones of Bel'kovsky Island grouped around 93 Ma (Fig. 7a). AHe ages obtained from the Devonian and Permian sandstones of Bel'kovsky Island (12 AP33, 12AP20, 8-va-12-13) group in the latest Cretaceous between 85–104 Ma. Fifteen AHe ages from the Oligocene strata of Bel'kovsky Is. are older than depositional ages, suggesting exhumation of the provenance area. Most of the ages average around 100 Ma (Fig. 7b).

2.3.3.1.1. Thermal modelling of (U-Th)/He data. Inverse thermal history modelling for Bel'kovsky Island was performed on three grains from sample 8-va-12-13, and model results allow for a broad range of maximum temperatures prior to a protracted cooling history from the Early Cretaceous to present (Fig. 24A). Forward models test the effects of increasing burial temperature from 100 to 200 °C on expected AHe date-eU trends in samples 8-va-12-13 and 12AP20 (Fig. 24B). With the exception of a single date, these models replicate the observed AHe date dispersion at all temperatures, suggesting that observed AHe date-eU trends are controlled by the cooling history of the samples. Modelled ZHe date-eU inheritance envelopes are compared with ZHe dates from Bel'kovsky, and the adjacent Kotel'nyi Island (Fig. 24C). Forward models indicate that temperatures of 100 °C cannot account for much of the observed ZHe data, whereas 200 °C results in too restrictive an inheritance envelope. Of the three examples, the 150 °C model best encompasses both the partially and fully reset ZHe dates. However, even the 150 °C forward model is unable to account for the majority of the young (79–105 Ma) ZHe dates. These dates present an interesting challenge to thermal history modelling, as they are the same age or younger than many of the AHe dates from the same sample, as well as AHe dates from the other Devonian and Permian samples from Bel'kovsky Island. A similarity in AHe and ZHe dates should require a rapid Late Cretaceous cooling event. However, the ZHe dates highlight the complications of correlating radiation damage annealing models for apatite (Flowers et al., 2009) and zircon (Guenthner et al., 2013) for partially reset detrital samples, and leave open the possibility of a rapid Late Cretaceous cooling event on Bel'kovsky and Kotel'nyi islands.

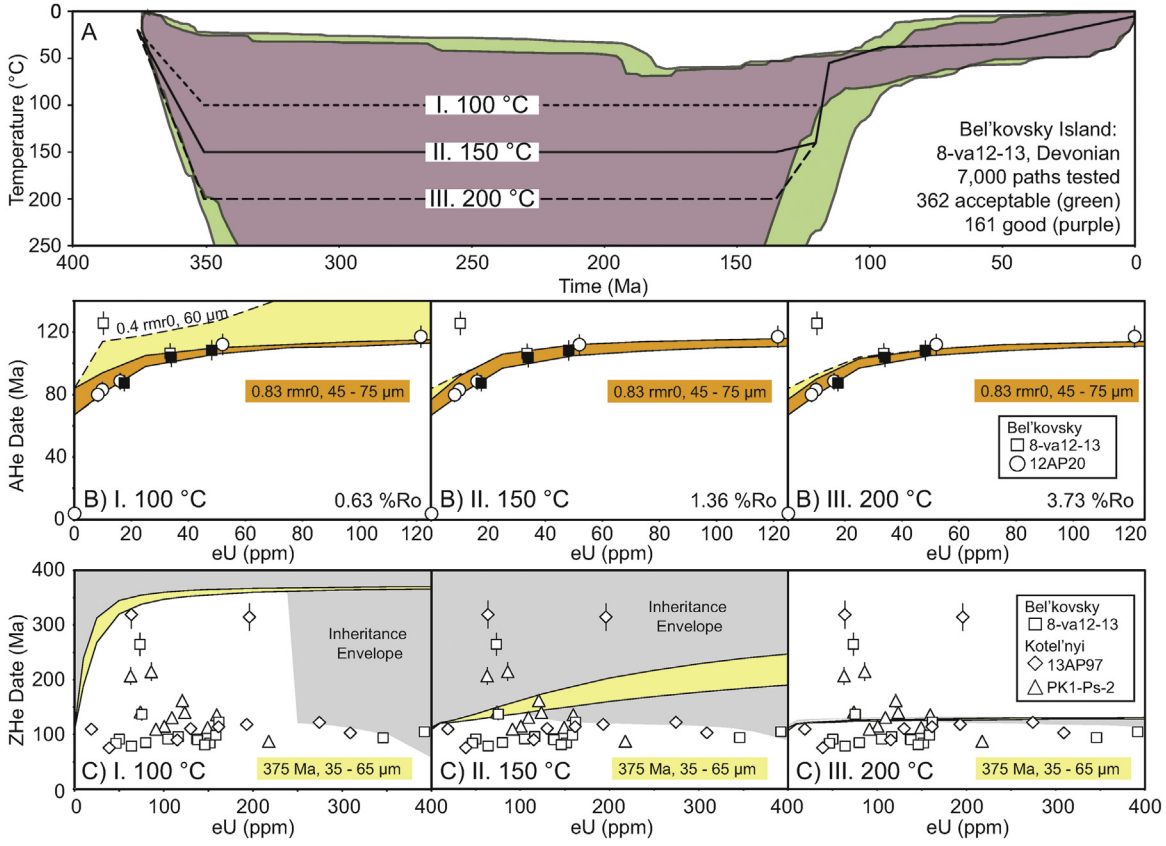

Fig. 24. Thermal history models for data from Bel'kovsky and Kotel'nyi islands. (A) Inverse thermal history model for sample 8-va-12-13, as well as three t-T histories (I, II, III) invoked in forward modelling. (B) AHe forward models for 8-va-12-13 and 12AP20. Models show probable date-eU trends for a range of grain size and annealing kinetics (rmr0: Carlson et al., 1999; Ketcham et al., 2007). Apatite dates in black indicate data incorporated into the inverse thermal history model. (C) ZHe forward models that highlight the expected "inheritance envelope" (Guenthner et al., 2015) that encompasses modelled ZHe date-eU trends for all possible pre-depositional histories in the detrital zircon population. ZHe data are plotted for both Bel'kovsky and Kotel'nyi islands. (For interpretation of the references to colour in this figure legend, the reader is referred to the web version of this article.)

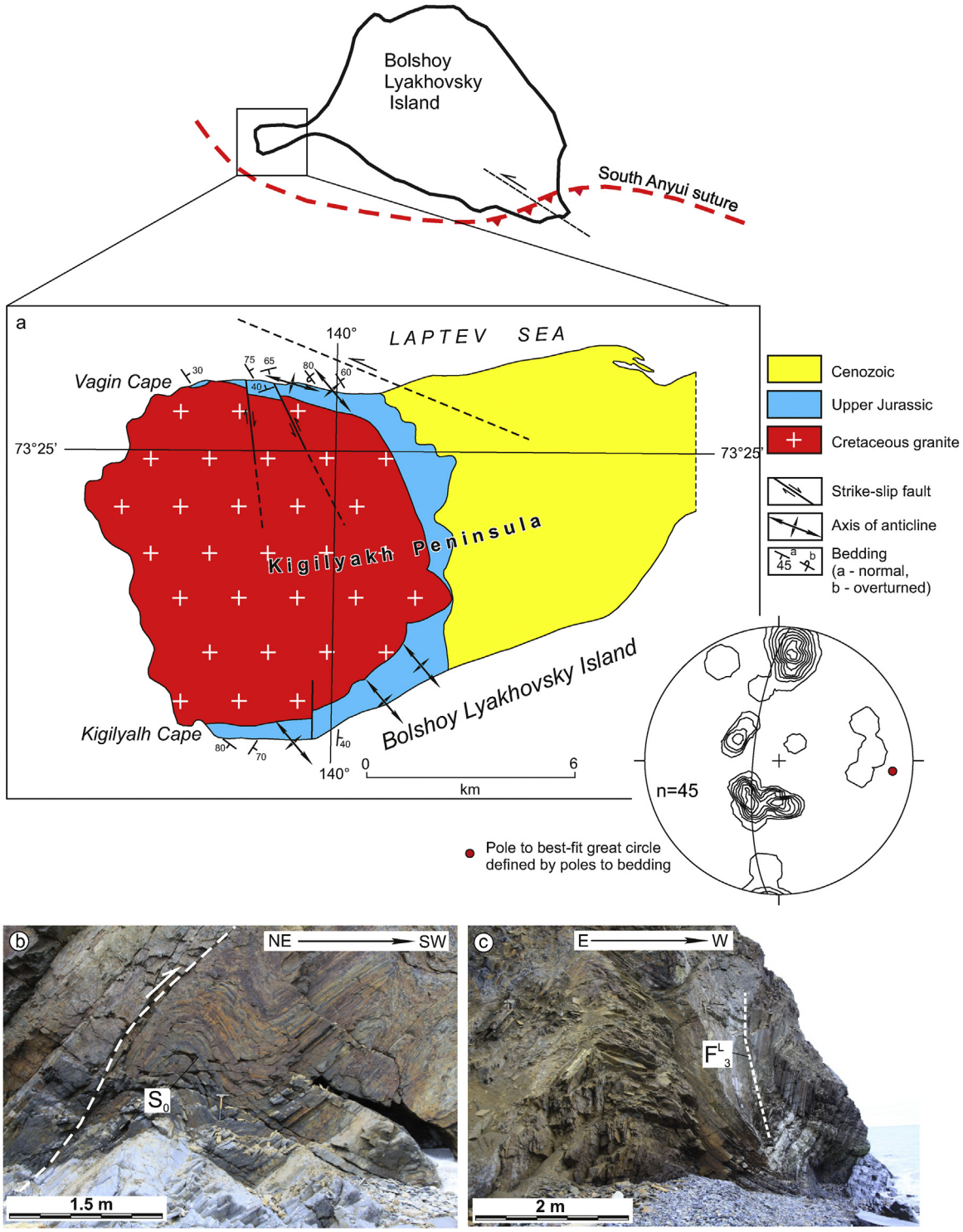

Fig. 25. (a) Simplified geological map of Kigilyakh Peninsula (Bolshoy Lyakhovsky Island) (modified from Samusin and Belousov, 1985) and pole to bedding diagram (equal-area projection, lower hemisphere; n – number of measurements); (b) NW-SE trending F_1^L folds of the first generation (D_1^L); (c) folds F_3^L with steeply dipping axes within the Upper Jurassic rocks. (For interpretation of the references to colour in this figure legend, the reader is referred to the web version of this article.)

2.4. Lyakhovsky Islands

2.4.1. Structural studies of Bolshoy Lyakhovsky Island (northern coast of the Kigilyakh Peninsula)

Upper Jurassic sandstones and siltstones are draped into NW-SW trending F_1^L folds of the first generation (D_1^L), overturned to the SW (Samusin and Belousov, 1985). Their trend is the same as the folds of F_2^K on Kotel'nyi Island. However, our observations in the north of the peninsula show that the axes of these folds are probably turned counterclockwise to the west during the second deformation stage, D_2^L (Fig. 25a). Here, their axes plunge to the WNW and ESE (Fig. 25, diagram). These folds are concentric and cylindrical, with a width and scale from a few decimeters to a few tens of meters. Cleavage is absent. The folds are associated with small-scale reverse faults (Fig. 25b). The rocks are intruded and metamorphosed by Cretaceous granites dated at 106 Ma (Layer et al., 2001). The map (Fig. 25a) shows that in the north

of the peninsula, the granites and Jurassic deposits are deformed by sinistral and dextral strike-slip faults trending ~N-S (Samusin and Belousov, 1985). However, we observed here only dextral faults with a reverse slip component and a NNW-SSE trend. The orientation of these strike-slip faults is the same as dextral strike-slip faults observed on Kotel'nyi Island. These faults formed during the D_3^L deformation stage, and the folds of F_3^L with steeply dipping axes within the Upper Jurassic deposits are associated with them (Fig. 25c).

In the southeast of Bolshoy Lyakhovsky Island, an ophiolite complex is exposed including serpentinites, Late Jurassic oceanic basalts, amphibolites, dunites, peridotites, and blueschists (Drachev, 1989; Drachev and Savostin, 1993; Drachev et al., 1998; Kuzmichev, 2009). The complex extends along the strike of the South Anyui suture, which here bends and has a NE-SW strike (Shalaurov terrane after Nokleberg et al., 2001; Parfenov et al., 1993b; Parfenov and Kuz'min, 2001). Oceanic rocks were thrust on Late Jurassic-Early Cretaceous and/or Late Triassic shale and sandstone in a NW direction during the first deformation stage (D_1^L). In the second deformation stage (D_2^L), in accordance with A. Kuzmichev's geological map (2009), it can be assumed that NW-SE sinistral strike-slip faults were formed. The rocks are intruded by granitoids as old as 121-114 Ma (Kuzmichev, 2009), with ^{40}Ar-^{39}Ar cooling ages of 113-105 Ma (Layer et al., 2001).

The observed differences between strikes of D_1^L deformations in the west and southeast of the island can be explained by the change in the direction of the strike of the South Anyui suture. Sinistral strike-slip faults located in the southeast of the island could be the cause of the bending of the fold axes of F_1^L in the west to the Kigilyakh Peninsula.

3. Discussion

Reconstructing the tectonic evolution of the NSI and adjacent parts of the East Siberian and Laptev Sea shelves is complicated because of the scattered distribution of outcrops across the archipelago and incompleteness of preserved stratigraphy. The correlation of tectonomagmatic events across the NSI is shown in Fig. 26. The oldest strata preserved across the NSI are Ediacaran and Cambrian volcaniclastic rocks, cropping out on Henrietta and Jeannette islands. The Ediacaran part of the succession on Henrietta Island is intruded by Ediacaran mafic dykes (Prokopiev et al., 2017), which mark the oldest magmatic event across the study region. Ediacaran-Cambrian volcaniclastic rocks and Ediacaran dykes were deformed by thrusts of the first deformation stage (D_1^H) in the Late Cambrian, and are overlain by Late Cambrian basalts. Deformations of the second stage (D_2^H) on Henrietta Island involved the development of strike-slip faults with a reverse slip component, which displaced both the Ediacaran-Cambrian succession and Late Cambrian basalts. So, the age of D_2^H on Henrietta Island is post-Late Cambrian.

The Upper Cambrian volcaniclastic succession cut by thrusts and metamorphosed during D_1^J deformation stage is exposed on Jeannette Island and intruded by Late Cambrian mafic dykes. Thus, the age of the deformation stage D_1^H on both Jeannette and Henrietta islands is Late Cambrian. Deformations of the second stage described on Henrietta Island were not detected on Jeannette Island.

However, the coeval Cambrian-Ordovician strata on Bennett Island represent the exposed fragment of a shallow marine shelf. The oldest deposits reported from the Anjou Islands are mostly carbonates of the Ordovician succession. Thus, the Late Cambrian basaltic magmatism and the Ediacaran–Cambrian volcaniclastic deposits are interpreted as forming in an arc-backarc tectonic setting (Ershova et al., 2016a) in the area of the present Henrietta and Jeannette islands. The western parts of the NSI are dominated by a shallow marine sedimentary succession, which was deposited during a period of tectonic quiescence. The Silurian to Middle Devonian succession is only known from Kotel'nyi Island and comprises mainly carbonates with subordinate beds of clastic deposits (Ershova et al., 2016b; Kos'ko et al., 1985). There is no evidence for tectonic or magmatic activities observed within this time slice.

Ershova et al. (2016a) proposed that the De Long Islands together with other continental blocks, such as Severnaya Zemlya and Arctic Alaska–Chukotka, formed the contiguous active continental margin of Baltica during the early Paleozoic. Henrietta and Jeannette islands are thought to have been part of an active continental margin in the early Paleozoic, which was separated by a back-arc basin from the shallow marine shelf (Bennett Island) (Ershova et al., 2016a). The early-middle Paleozoic rocks of Kotel'nyi Island most likely formed part of this shelf, although rocks older than Ordovician are not exposed here.

Folding and faulting of the D_1^J stage on Jeannette Island and D_1^H stage on Henrietta Island show similar W-to WSW-transport directions, indicating that exposed structures belong to the same tectonic domain. Rocks exposed on Jeannette Island are metamorphosed to greenschist facies and are more intensely deformed than on Henrietta Island. The character and orientation of the deformation structures on both islands suggest that they formed part of a single early Paleozoic orogenic belt, whose central part is submerged beneath the East Siberian Sea. Based on the intensity of deformation, it can be assumed that Jeannette Island folded complexes are located closer to the central part of this orogen than coeval deposits of Henrietta Island.

The next tectonic event clearly seen from the oldest ZHe ages on the De Long archipelago indicates 5–6 km of uplift and erosion in Devonian time. The oldest ZHe ages (378 ± 38 Ma on Bennett Island, 398 ± 22 Ma on Henrietta Island, and 414 ± 15 Ma on Jeannette Island) reasonably correlate with the deformation stage D_1^K and the pre-Frasnian angular unconformity on Kotel'nyi Island. This event could be associated with intrusions of basaltic trachyandesite sills (419.2 ± 3.7Ma, $^{40}Ar/^{39}Ar$) (Ershova et al., 2016a) and mafic dykes, which intruded into Late Cambrian basalts on Henrietta Island. We assume that deformations of D_2^H on Henrietta Island also occurred at this time. This suggests that the NSI belonged to a single Devonian orogenic belt, forming the D_1^K contractional deformation stage on Kotel'nyi Island and the broad anticline on Bennett Island (D_1^B).

Thus, the observed mid-Paleozoic deformation can be used to refine existing plate tectonic models of the study region. During the Devonian, the northern part of Siberia was affected by an extensional (rifting) regime as opposed to a contractional one (Parfenov and Kuz'min, 2001). Therefore, our data on the compressional stress regime deduced from structural data from the Anjou Islands and low-temperature dates from the De Long Islands support tectonic models claiming a non –Siberian affinity of the NSI during the mid-Paleozoic (e.g. Drachev et al., 2011; Dumoulin et al., 2002; Ershova et al., 2015a, b; Ershova et al., 2016a,b). According to these models, the NSI represents a part of the Arctic Alaska-Chukotka microcontinent (e.g. Drachev et al., 2011).

Based on the direction of tectonic transport, contraction occurred from north to south (in present-day coordinates) on Kotel'nyi Island at the boundary between the Middle and Late Devonian. The small scale of the structures suggests that the Anjou and De Long islands formed a distal part of an orogenic belt in the middle Paleozoic.

There is abundant evidence for circum-Arctic mid-Paleozoic contractional deformation events. These include the Early Devonian to earliest Middle Devonian Romanzof Orogeny, reported across northwestern Yukon, northeastern Alaska and the North Slope of Alaska (e.g. Lane, 2007). Late Devonian to Early Carboniferous deformations characterizing the Ellesmerian Orogeny or Svalbardian event of the Caledonides are described from many localities across the Arctic realm, including Arctic Alaska (e.g. Lane, 2007), the Canadian Arctic (e.g. Embry, 1988; Piepjohn et al., 2008), northern Greenland (e.g. Soper and Higgins, 1990), Svalbard (Svalbardian Orogeny) (e.g. Kośmińska et al., 2016; McCann, 2000; Piepjohn, 2000; Piepjohn et al., 2008, 2015; Rippington et al., 2010), Wrangel Island (Verzhbitsky et al., 2014, 2015) and the Chukchi Borderland (O'Brien et al., 2016).

Therefore, an angular pre-Frasnian unconformity observed on Kotel'nyi Island and significant exhumation revealed by low-temperature dates across the De Long Islands, suggest that Middle Devonian tectonism was widespread across the study area. Our data strongly

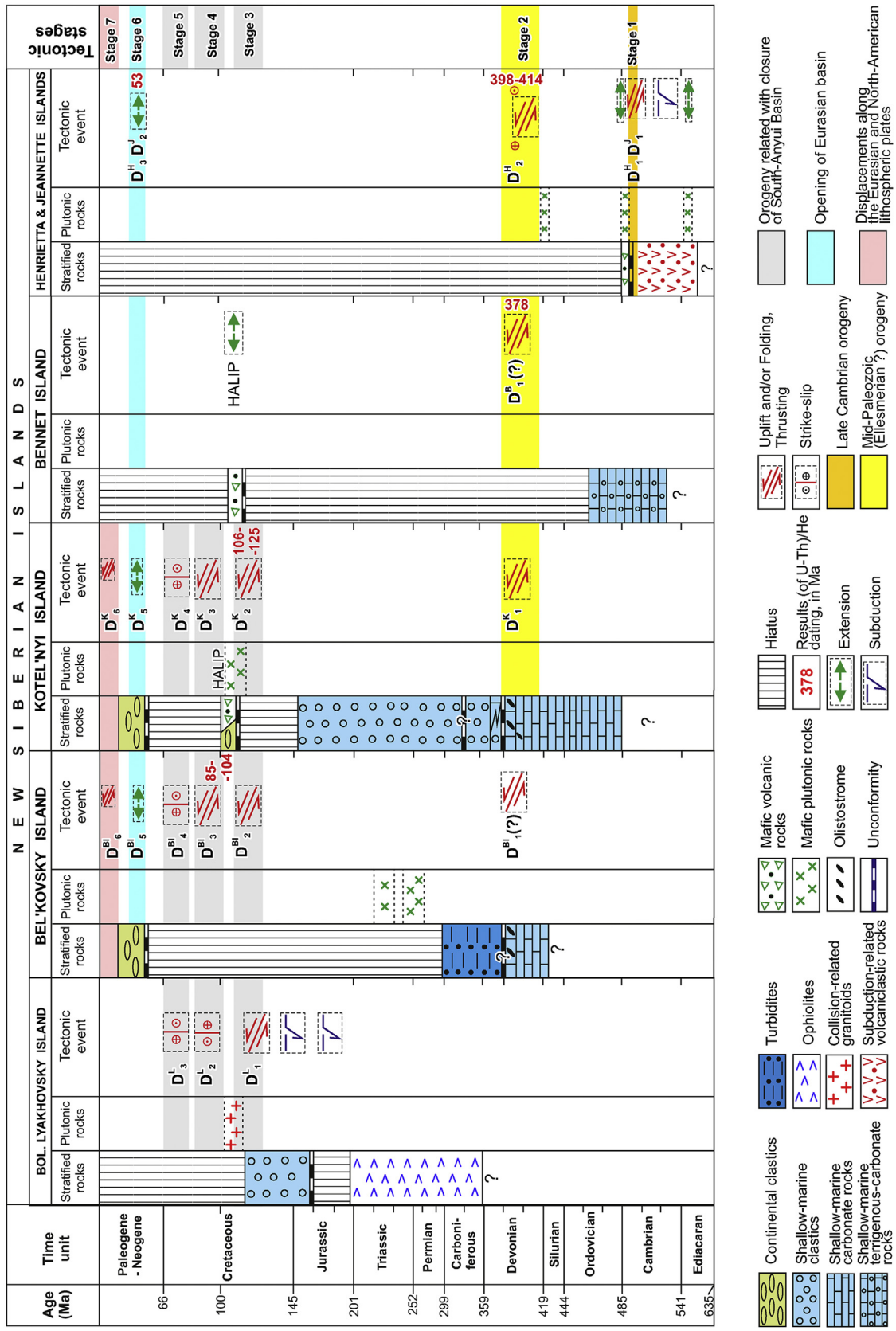

Fig. 26. Correlation of tectonic and magmatic events across the NSI. See text for discussion. (For interpretation of the references to colour in this figure legend, the reader is referred to the web version of this article.)

support models claiming a non –Siberian affinity of the NSI (e.g. Drachev et al., 2011; Ershova et al., 2015a,b, 2016a,b), and furthermore, suggest a possible affinity of the NSI with the Arctic Alaska–-Chukotka microcontinent (e.g. Ershova et al., 2017; Grantz et al., 1990; Lawver et al., 2002; Miller et al., 2006; Natal'in et al., 1999; Nokleberg et al., 2001; Sengo¨r and Natal'in, 1996 and references therein). This is inconsistent with models based on biostratigraphic correlation of Paleozoic sequences of the NSI, assuming that in the early-middle Paleozoic the NSI were linked to the Siberian continent (e.g. Kos'ko and Korago, 2009; Kuzmichev, 2009; Danukalova, 2016). Our data also contradict paleomagnetic studies (Metelkin et al., 2014, 2015; Vernikovsky et al., 2013) claiming that the NSI were a separate terrane during the Paleozoic, with no connection to larger continental landmasses. Based on the preserved sedimentary succession of Kotel'nyi Island, the Late Devonian to Late Jurassic, at least in the western part of the study region, was occupied by shallow marine (Kotel'nyi Island) to deep marine (Bel'kovsky Island) depositional environments. The Permian/Triassic boundary and Middle Triassic were marked by short episodes of mafic magmatism, manifested by dykes and sills observed across Bel'kovsky Island (Kuzmichev and Pease, 2007; Prokopiev et al., 2017).

The next prominent tectonic event across the study region occurred at the latest Early Cretaceous to Late Cretaceous, deduced from thermochronological data obtained from the Anjou Islands. However, this event has not been reported from the De Long Islands. This event led to formation of the modern structures on Kotel'nyi and Bel'kovsky islands, creating the D_2^K and D_2^{Bl} contractional deformation structures along with intensive uplift and rapid erosion. On Bolshoy Lyakhovsky Island, this stage is manifested by formation of folding and thrusts D_1^L, and associated with closure of the South Anyui Ocean and formation of the suture. It is marked by the presence of an angular unconformity between deformed Paleozoic-Jurassic (?) deposits and Aptian-Albian clastics and ignimbrites in the central part of Kotel'nyi Island (Kos'ko et al., 1985; Kuzmichev et al., 2009). However, the ages of these Cretaceous weakly deformed strata of Kotel'nyi Island are not precisely established. The fossil flora suggest an Aptian-Albian age, however K-Ar dates of the ignimbrites vary from 110 to 102 Ma (Kuzmichev et al., 2009). Therefore, these sediments could represent the erosional products of a coeval orogen, which was formed as a result of the collision of the Arctic Alaska-Chukotka microcontinent with the northern margin of Siberia. The Aptian-Albian deposits in the central part of Kotel'nyi Island are deformed into an asymmetric ~N-S trending syncline, with a steeper eastern limb indicating tectonic transport occurred from east to west. These deformations of D_3^K and D_3^{Bl} are manifested in the west of Kotel'nyi Island and on Bel'kovsky Island while simultaneous sinistral strike-slip movements of D_2^L stage occurred almost parallel to the South Anyui suture at Bolshoy Lyakhovsky Island, which could induce the contractional deformations of D_3 stage on the Anjou islands. This allows us to assume that the Arctic Alaska-Chukotka microcontinent was moving at that time in the western direction (modern coordinates).

Post-Aptian-Albian deformations also include dextral strike-slip faults of a N-S-trend (D_4^K stage), displacing Albian volcaniclastic rocks in the central part of Kotel'nyi Island and manifested on Bel'kovsky Island (D_4^{Bl}) and Bolshoy Lyakhosvsky Island (D_3^L). These deformations mark the displacement of the Arctic Alaska-Chukotka microcontinent in a southern direction (modern coordinates) during this time.

The AHe and ZHe ages obtained from Bel'kovsky Island are slightly younger than those from Kotel'nyi Island, however, all ages fall within analytical error. Two models can be proposed to explain these ages. The first model claims that rapid uplift and erosion occurred simultaneously across the islands, resulting in all ages lying within analytical error. However, a younging of ZHe and AHe ages from the east (Kotel'nyi Island) to the west (Bel'kovsky Island) is observed, and ZHe ages in the western part of Bel'kovsky Island (12AP33 sample) are approximately 10 Ma younger than ZHe and AHe ages from the eastern part of the island (12AP20, 8-va-12-13). Thus, a second speculative tectonic model can be generated, whereby uplift occurred relatively simultaneously across Kotel'nyi and Bel'kovsky islands with similar erosion rates, however, a thicker portion of sediments were eroded across Bel'kovsky Island, leading to a slightly later resetting of ZHe and AHe ages in a westward direction. This implies that in the western part of the NSI, a thicker succession of Permian-Jurassic strata was possibly completely eroded during Cretaceous uplift. This idea is partly supported by a facies transition from the shallow marine relatively thin Devonian-Permian strata of Kotel'nyi Island, to relatively deep marine and thicker coeval strata of Bel'kovsky Island (Ershova et al., 2016b). This latest Early Cretaceous – early Late Cretaceous deformation event across the NSI, accompanied by significant uplift, coincides with the timing of closure of the South Anyui/Angayucham Ocean and formation of the South Anyui suture. Several scenarios have been proposed for the formation of the suture (e.g. Parfenov, 1984; Natal'in, 1984; Sengo¨r and Natal'in, 1996; Sokolov et al., 2015; Nokleberg et al., 2001; Amato et al., 2015; Piepjohn et al., 2017). The late Paleozoic-Early Cretaceous South Anyui/Angayucham Ocean basin separated the Siberian craton and Kolyma-Omolon superterrane or microcontinent from the Arctic Alaska-Chukotka microcontinent. Closure of the ocean took place in Aptian-early Albian times (Parfenov and Kuz'min, 2001), or before the Aptian collision (Sokolov et al., 2015). The South Anyui suture (accretionary wedge terrane after Nokleberg et al., 2001; Parfenov and Kuz'min, 2001; suture zone after Seslavinsky, 1979) is situated between the northern margin of the Kolyma-Omolon superterrane and the southern margin (modern coordinates) of the Arctic Alaska-Chukotka microcontinent. It can be traced northwestwards over 400 km under the cover of Cenozoic deposits, from the lower reaches of the Kolyma River to the shore of the East Siberian Sea, by linear magnetic and gravity anomalies (Spektor et al., 1981). Ophiolites associated with the suture zone are exposed in the east of Bolshoy Lyakhovsky Island (e.g. Parfenov and Kuz'min, 2001; Kuzmichev, 2009). The westward continuation of the South Anyui suture across the Laptev Sea is still a matter of discussion. We share the opinion of Franke et al. (2008) and Brandes et al. (2015) that it can be followed from Bolshoy Lyakhosvsky Island north-north-westwards to the east of Stolbovoy Island and further northward to the west of Bel'kovsky Island (Fig. 27). The age of the collision is also supported by the presence of 121 Ma (U-Pb, zircon) and 113 Ma ($^{40}Ar/^{39}Ar$, mica) granitic intrusions on Bolshoy Lyakhovsky Island (Kuzmichev, 2009; Layer et al., 2001).

Therefore, we relate the latest Early–Late Cretaceous thermal event to the closure of the South Anyui/Angayucham Ocean, accompanied by simultaneous uplift across the NSI during the formation of an orogenic belt. The absence of a similar deformation event on the De Long Islands is likely to be due to their distal location relative to the suture zone.

Our study supports tectonic models claiming that Mesozoic tectonism across the NSI was caused by closure of the South Anyui Ocean (Drachev et al., 2010), manifested by the formation of the Novosibirsk-Chukotka orogenic belt between Siberia and the Arctic-Alaska Chukotka microcontinent during the latest Early Cretaceous. We suggest that the NSI formed a part of the Arctic-Alaska Chukotka microcontinent and can be interpreted as an indenter. The D_2^K- D_2^{Bl} tectonic event is characterized by the formation of folds and thrusts with a NW-SE trend along the western margin of the NSI (Kotel'nyi and Bel'kovsky islands), along with folds and thrusts with WSW-ENE and NW-SE trends along its southern margin (Bolshoy Lyakhovsky Island) (D_1^L). In the west of Bolshoy Lyakhovsky Island, the trend of folding during the D_1^L stage is the same as during the D_2^K and D_2^{Bl} stages on the Anjou Islands. A contrasting folding trend reported from the southeast of Bolshoy Lyakhovsky Island could be explained by the curved configuration of the South Anyui suture in that area. Subsequent sinistral strike-slip motions along the southern part of the South Anyui suture (Bolshoy Lyakhovsky Island) (D_2^L) led to the formation of ~ N-S trending shortening across the Anjou Islands (D_3^K, D_3^{Bl}). During the final stage, the Arctic-Alaska Chukotka microcontinent indenter moved southward, and dextral strike-slip faults (stages D_4^K, D_4^{Bl}, D_3^L) formed in the west of the Anjou

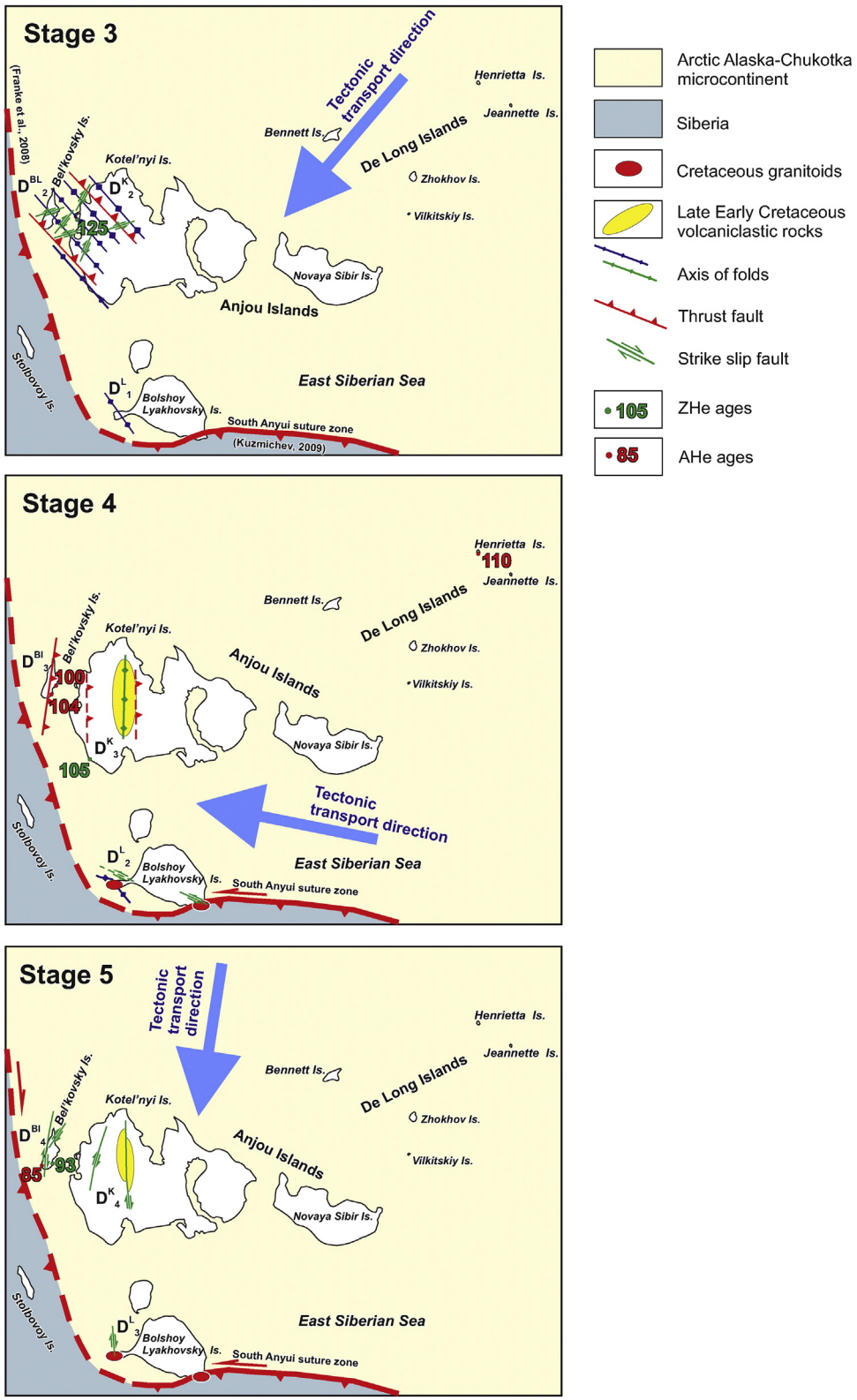

Fig. 27. Proposed model of Mesozoic deformation events (stages 3–5, see Fig. 26) across the NSI with weighted average ZHe and AHe ages illustrated the Mesozoic episodes of uplifts. See text for discussion. (For interpretation of the references to colour in this figure legend, the reader is referred to the web version of this article.)

Islands and in the west of Bolshoy Lyakhovsky Island (Fig. 27). Furthermore, such a scenario explains the lack of intensive deformation across the De Long Islands, due to their location in the interior part of the Arctic-Alaska Chukotka microcontinent.

Thus, we assume that the Mesozoic deformations on the Anjou and Lyakhovskiy islands mark the southwestern part of the Novosibirsk-Chukotka late Mesozoic orogenic belt that formed as a result of closure of the South Anyui Ocean. Northern continuation of this orogenic belt is covered by the East Siberian Sea that makes impossible reasonable estimation of it distribution. The northern limit of this orogenic belt likely

coincides with the Wrangel-Herald fault mapped by seismic data. To the north from it, the New Siberian-Wrangel foreland basin presumably filled in with the Late Jurassic to Early Cretaceous deposits is identified by seismic data (e.g. Drachev et al., 2010; Drachev, 2016). The Novosibirsk-Chukotka orogenic belt, like the South Anyui suture, extends far to the east and is exposed in western Chukotka, where ophiolites, contractional and subsequent strike-slip deformations have been described (e.g. Natal'in, 1984; Sokolov et al., 2009, 2015 and references therein).

The next episode of mafic magmatism reported from the study region is related to the ca. 106–124 Ma basalts reported from Bennett Island (De Long Islands) (Drachev, 1999; Fedorov et al., 2005). These mafic rocks have been interpreted as evidence for the spread of HALIP magmatism across the study region (Drachev and Saunders, 2006).

The Cenozoic tectonic event (D_5^K, D_5^{Bl}) corresponds to the opening of the Eurasian Basin and is marked by development of an extensional regime across the study area, manifested by the widespread distribution of younger normal faults displacing older contractional structures. This event led to the formation of small grabens and depressions across the Anjou Islands. For example, on Bel'kovsky Island, there is a graben filled with 40 m-thick Late Eocene to Early Miocene continental deposits with a weathering crust at the base (Kos'ko et al., 1985; Kuzmichev et al., 2013). The AHe ages obtained from the Cambrian rocks of Jeannette Island average at ca. 53 Ma and are close to the time of initial sea-floor spreading in the Eurasian Basin. An extensional stress regime was widely distributed across the neighboring Laptev Sea shelf, manifested by numerous grabens presumably mainly filled by Cenozoic sediments (e.g. Drachev, 2016; Franke et al., 2008; Franke and Hinz, 2005 and references therein).

The cause of contractional deformations affecting the Cenozoic deposits of the Anjou Islands (D_6^K, D_6^{Bl}) is unclear, but it can be assumed that they are associated with motions along the Eurasian and North-American lithospheric plates.

The youngest magmatic event across the study region is reported from the De Long Islands (Vil'kitskiy and Zhokhov islands), and manifested by Quaternary (ca. 1.2 Ma) basaltic volcanism (Layer et al., 1993).

The youngest deformations reported from the study region are caused by glacio-tectonics during regional glaciation in the second half of the middle Pleistocene. The glacial deformation of Upper Cretaceous and Pleistocene (?) sediments are described on Novaya Sibir Island (Danukalova and Kuzmichev, 2014; Piepjohn et al., 2017).

4. Conclusions

A: Our structural studies reveal the following succession of major stages of contractional and extensional deformations across the NSI:

Stage 1: The earliest deformations occurred in the east of the De Long Islands in the Late Cambrian (D_1^H and D_1^J). This area was presumably located in close proximity to an early Paleozoic orogenic belt.

Stage 2: An angular unconformity at the base of the Middle Frasnian deposits represents an episode of contractional deformation, with folds and S-SW-diping thrusts reported across the western Kotel'nyi Island (Anjou Islands) (D_1^K). The strike-slip faults with a reverse slip component (D_2^H) on the Henrietta Island and broad anticline on Bennett Island (D_1^B) (De Long islands) are possibly associated with this mid-Paleozoic tectonic event. This part of the NSI is likely to have formed a distal part of an orogenic belt in the middle Paleozoic, which may be correlated with one of the phases of the Ellesmerian Orogeny.

Stage 3: The latest Early Cretaceous (Aptian?) stage was marked by the formation of major NW-SE trending folds, thrusts and transfer strike-slip faults across the Anjou Islands (D_2^K and D_2^{Bl}). Folding and thrusting (stage D_1^L) reported from Bolshoy Lyakhosvsky Island are also associated with this stage of deformation. This widely reported contractional event across the study region is associated with closure of the South Anyui/Angayucham Ocean, resulting in collision of the western part of the Arctic Alaska-Chukotka microcontinent with Siberia and forming the South Anyui suture zone and coeval orogenic belt. The youngest episode of stage 3 is characterised by accumulation of Aptian-Albian volcaniclastic rocks in the central part of Kotel'nyi Island, along with the emplacement of synchronous granitoids at Bolshoy Lyakhovsky Island.

Stage 4: In post-Aptian time, formation of the orogenic belt continued. The Arctic Alaska-Chukotka microcontinent moved westward. On Bolshoy Lyakhovsky Island, along the South Anyui suture, sinistral strike-slip fauls (D_2^L) were formed. On the Anjou islands, E-W compression (D_3^K and D_3^{Bl}) resulted in deformation of Aptian-Albian deposits in the central part of Kotel'nyi Island.

Stage 5: The Arctic Alaska-Chukotka microcontinent moved in a southern direction. N-S-trending dextral strike-slip faults were formed, displacing Aptian-Albian volcaniclastic rocks in the central part of Kotel'nyi Island (D_4^K), also manifested on Bel'kovsky Island (D_4^{Bl}) and in the west of Bolshoy Lyakhosvsky Island (D_3^L). This stage marked the final phase of formation of the Novosibirsk-Chukotka orogenic belt.

Stage 6: The Cenozoic extensional event (D_5^K, D_5^B) corresponds to opening of the Eurasian Basin.

Stage 7: The late Cenozoic contractional deformation event reported from the Cenozoic deposits of the Anjou Islands (D_6^K, D_6^{Bl}) were likely to have been caused by displacements along the Eurasian and North-American lithospheric plates.

B: Thermochronologic analyses of 12 samples from different islands of the NSI were carried out. The ZHe analysis of Cambrian rocks of the De Long Islands suggests exhumation of at least 5–6 km of sediment in the eastern portion of the NSI at ca. 378–414 Ma, and can be correlated with the angular unconformity at the base of the Frasnian observed in the western part of Kotel'nyi Island. The latest Early - Late Cretaceous (ca. 93–125 Ma, AHe, ZHe) cooling episode, established in the west of the NSI (Anjou Islands), indicates a significant episode of uplift, which occurred during the final stages of closure of the South Anyui Ocean and coeval formation of the South Anyui suture and orogenic belt. The Cenozoic low-temperature thermochronologic data (ca. 53 Ma, Early Eocene, AHe), which is recorded in the eastern part of the NSI (Jeannette Island), corresponds to the opening of the Eurasian basin.

C: Our new data support a non-Siberian affinity of the NSI and an affinity with the Arctic Alaska–Chukotka microcontinent.

Acknowledgments

The study was partially supported by project IX.124.1. (no. 0381-2016-0001) from the Diamond and Precious Metal Geology Institute, and project 53 of program 44P from the Presidium of the Russian Academy of Sciences. Structural data processing and interpretation were supported by grant no. 17-17-01171 by the Russian Science Foundation. Fieldworks were performed with support of VSEGEI and in the framework of the joint project of TGS Nopec Co. and Clapton Research. VE, OA and DS were partly supported by the Research Council of Norway grant 254962/H30, RCN project Changes at the Top of the World through Volcanism and Plate Tectonics: A Norwegian-Russian-North American collaboration in Arctic research and education: NOR-R-AM (no. 261729). Thanks to the UTChron geoanalytical staff and the University of Texas at Austin for laboratory support. Authors are grateful to James Barnet for useful comments and correcting the English. We thank two anonymous reviewers for their constructive comments, suggestions and corrections, which very much helped to improve the manuscript.

Appendix A. Supplementary data

Supplementary material related to this article can be found, in the online version, at doi:https://doi.org/10.1016/j.jog.2018.09.001.

References

Allmendinger, R.W., Cardozo, N.C., Fisher, D., 2012. Structural Geology Algorithms: Vectors & Tensors. Cambridge University Press, Cambridge, England 302 p.

Amato, J.M., Toro, J., Akinin, V.V., Hampton, B.A., Salnikov, A.S., Tuchkova, M.I., 2015. Tectonic evolution of the Mesozoic South Anyui suture zone, eastern Russia: a critical component of paleogeographic reconstructions of the Arctic region. Geosphere 11, 1530–1564. https://doi.org/10.1130/GES01165.1.

Barbarand, J., Carter, A., Wood, I., Hurford, T., 2003. Compositional and structural control of fission-track annealing in apatite. Chem. Geol. 198, 107–137. https://doi.org/10.1016/S0009-2541(02)00424-2.

Basilyan, A.E., Anisimov, M.A., Nikolskiy, P.A., 2009. The glaciation of the New Siberian Islands: the determining factor of the geological structure of the quaternary deposits. Geology of the Polar Regions of the Earth, Proceedings of XLII Tectonic Meeting, GEOS, Moscow 1, 43–45 (in Russian).

Basilyan, A.E., Nikolskiy, P.A., Maksimov, F.E., Kuznetsov, V.Yu., 2010. Age of cover glaciation of the New Siberian islands based on 230Th/U-dating of mollusk shells. The Structure and History of the Development of the Lithosphere, Paulsen, Moscow 506–514 (in Russian).

Beucher, R., Brown, R.W., Roper, S., Stuart, F., Persano, C., 2013. Natural age dispersion arising from the analysis of broken crystals. Part II: practical application to apatite (U-Th)/He thermochronometry. Geochim. Cosmochim. Acta 120, 395–416. https://doi.org/10.1016/j.gca.2013.05.041.

Brandes, C., Piepjohn, K., Dieter, F., Sobolev, N., Gaedicke, C., 2015. The Mesozoic–Cenozoic tectonic evolution of the New Siberian Islands, NE Russia. Geol. Mag. 152 (03), 480–491. https://doi.org/10.1017/S0016756814000326.

Brown, R.W., Beucher, R., Roper, S., Persano, C., Stuart, F., Fitzgerald, P., 2013. Natural age dispersion arising from the analysis of broken crystals. Part I: theoretical basis and implications for the apatite (U-Th)/He thermochronometer. Geochim. Cosmochim. Acta 122, 478–497. https://doi.org/10.1016/j.gca.2013.05.041.

Carlson, W.D., Donelick, R.A., Ketcham, R.A., 1999. Variability of apatite fission-track annealing kinetics: I. Experimental results. Am. Mineral. 84, 1213–1223. https://doi.org/10.2138/am-1999-0901.

Chernova, A.I., Metelkin, D.V., Matushkin Yu, N., Vernikovsky, V.A., Travin, A.V., 2017. Geology and paleomagnetism of Jeannette Island (De Long Archipelago, Eastern Arctic). Russ. Geol. Geophys. 58, 1001–1017.

Danukalova, M.K., 2016. Geological history of Bennett and Kotel'nyi Islands in the Early Paleozoic. PhD Thesis. (in Russian). .

Danukalova, M.K., Kuzmichev, A.B., 2014. Derevyannye gory (Novaya Sibir Island): fold-thrust thrust of the neopleistocene age. Proceedings of XLVI Tectonic Meeting, GEOS, Moscow 1, 104–106 (in Russian).

Djimbi, M.D., Gautheron, C., Roques, J., Tassan-Got, L., Gerin, C., Simoni, E., 2015. Impact of apatite chemical composition on (U-Th)/He thermochronometry: an atomistic point of view. Geochim. Cosmochim. Acta 167, 162–176. https://doi.org/10.1016/j.gca.2015.06.017.

Dorofeev, V.K., Blagoveshchenskiy, M.G., Smirnov, A.N., Ushakov, V.I., 1999. The New Siberian Islands. Geology and Minerageny. VNII Okeanologiya, St. Petersburg (in Russian).

Drachev, S.S., 1989. Tectonics and mesozoic geodynamics of the New Siberian Islands area. Synopsis of Cand. Sci. Thesis. Moscow, 19 p. (in Russian).

Drachev, S.S., 1999. Tectonics of the rift continental margin of northeast Eurasia in the Arctic (Laptev and East Siberian Seas). Synopsis of Doct. Sci. Thesis. Institute of Lithosphere, RAN, Moscow (in Russian).

Drachev, S.S., 2002. On the basement tectonics of the Laptev Sea Shelf. Geotectonics 36 (6), 483–498.

Drachev, S.S., 2016. Fold belts and sedimentary basins of the Eurasian Arctic. Arktos 2, 21. https://doi.org/10.1007/s41063-015-0014-8.

Drachev, S., Saunders, A.D., 2006. The Early Cretaceous arctic lip: its geodynamic setting and implications for Canada Basin opening. In: Scott, R.A., Thurston, D.K. (Eds.), Proceedings of the Fourth International Conference on Arctic Margins ICAM IV. US Department of the Interior, pp. 216–223.

Drachev, S.S., Savostin, L.A., 1993. Ophiolites of Bol'shoi Lyakhovsky Island (New-Siberian islands). Geotektonika 3, 98–107 (in Russian).

Drachev, S.S., Savostin, L.A., Groshev, V.G., Bruni, I.E., 1998. Structure and geology of the continental shelf of the Laptev Sea, Eastern Russian Arctic. Tectonophysics 298, 357–393.

Drachev, S.S., Malyshev, N.A., Nikishin, A.M., 2010. Tectonic history and petroleum geology of the Russian Arctic Shelves: an overview. In: In: Vinning, B.A., Pickering, S.C. (Eds.), Petroleum Geology: From Mature Basins to New Frontiers – Proceedings of the 7th Petroleum Geology Conference, vol. 7. Geological Society, London, pp. 591–619. https://doi.org/10.1144/0070591.

Drachev, S.S., 2011. Tectonic setting, structure and petroleum geology of the Siberian Arctic offshore sedimentary basins. In: In: Spencer, A.M., Embry, A.F., Gautier, D.L., Stoupakova, A.V., Sorensen, K. (Eds.), Arctic Petroleum Geology, vol. 35. Geological Society, London, Memoirs, pp. 369–394.

Dumoulin, J.A., Harris, A.G., Gagiev, M., Bradley, D.C., Repetski, J.E., 2002. Lithostratigraphic, conodont, and other faunal links between lower Paleozoic strata in northern and central Alaska and northeastern Russia. In: Miller, E.L., Grantz, A., Klemperer, S.L. (Eds.), Tectonic Evolution of the Bering Shelf-Chukchi Sea-Arctic Margin and Adjacent Landmasses. GSA Special Paper 360, Boulder, Colorado, pp. 291–312.

Embry, A.F., 1988. Middle?Upper Devonian sedimentation in the Canadian Arctic Islands and the Ellesmerian Orogeny. In: In: McMillan, N.J., Embry, A.F., Glass, D.J. (Eds.), Devonian of the World, 2. Can. Soc. Pet. Geol. Mem. 14. pp. 15–27.

Ershova, V.B., Prokopiev, A.V., Khudoley, A.K., Sobolev, N.N., Petrov, E.O., 2015a. Detrital zircon ages and provenance of the Upper Paleozoic successions of Kotel'ny Island (New Siberian Islands Archipelago). Lithosphere 7, 40–45.

Ershova, V.B., Prokopiev, A.V., Khudoley, A.K., Sobolev, N.N., Petrov, E.O., 2015b. U/Pb dating of detrital zircons from Upper Paleozoic deposits of Bel'kovsky Island (New Siberian Islands): critical testing of Arctic tectonic models. Int. Geol. Rev. 57 (2), 199–210.

Ershova, V.B., Lorenz, H., Prokopiev, A.V., Sobolev, N.N., Khudoley, A.K., Petrov, E.O., Estrada, S., Sergeev, S., Larionov, A., Thomsen, T.B., 2016a. The De Long Islands: a missing link in unraveling the Paleozoic paleogeography of the Arctic. Gondwana Res. 35, 305–322.

Ershova, V.B., Prokopiev, A.V., Khudoley, A.K., 2016b. Devonian–Permian sedimentary basins and paleogeography of the Eastern Russian Arctic: an overview. Tectonophysics 691 (PA), 234–255. https://doi.org/10.1016/j.tecto.2016.03.026.

Ershova, V.B., Prokopiev, A.V., Sobolev, N.N., Petrov, E.O., Khudoley, A.K., Faleide, J.I., Gaina, C., 2017. New data on composition of basement of Franz Josef land archipelago. Geotectonics 51 (2), 121–130.

Ershova, V.B., Prokopiev, A.V., Andersen, T., Khudoley, A.K., Kullerud, K., Thomsen, T., 2018. U-Pb and Hf isotope analysis of detrital zircons from Devonian-Permian strata of Kotel'ny Island (New Siberian Islands, Russian Eastern Arctic): insights into the Middle-Late Paleozoic evolution of the Arctic. J. Geodyn. 119, 199–209.

Farley, K.A., 2000. Helium diffusion from apatite: general behavior as illustrated by Durango fluorapatite. J. Geophys. Res. 105, 2903–2914. https://doi.org/10.1029/1999JB900348.

Farley, K.A., 2002. (U-Th)/He dating: techniques, calibrations, and applications. Rev. Mineral. Geochem. 47, 819–844. https://doi.org/10.2138/rmg.2002.47.18.

Fedorov, P.I., Flerov, G.B., Golovin, D.I., 2005. New data on the age and composition of volcanic rocks of Bennett Island, Eastern Arctic. Dokl. Earth Sci. 400 (5), 666–670 (in Russian).

Flowers, R.M., Ketcham, R.A., Shuster, D.L., Farley, K.A., 2009. Apatite (U-Th)/He thermochronometry using a radiation damage accumulation and annealing model. Geochim. Cosmochim. Acta 73, 2347–2365. https://doi.org/10.1016/j.gca.2009.01.015.

Franke, D., Hinz, K., 2005. The structural style of sedimentary basins on the shelves of the Laptev Sea and western East Siberian Sea, Siberian Arctic. J. Pet. Geol. 28, 269–286.

Franke, D., Reichert, C., Damm, V., Piepjohn, K., 2008. The South Anyui suture, Northeast Arctic Russia, revealed by offshore seismic data. Nor. J. Geol. 88, 189–200.

Fujita, K., Stone, D.V., Layer, P.W., Parfenov, L.M., Kos'min, B.M., 1997. Cooperative program helps decipher tectonics of northeastern Russia. EOS Trans. AGU 76 (24), 252–253 245.

Gautheron, C., Tassan-Got, L., Barbarand, J., Pagel, M., 2009. Effect of alpha-damage annealing on apatite (U-Th)/He thermochronology. Chem. Geol. 266, 166–179. https://doi.org/10.1016/j.chemgeo.2009.06.001.

Gautheron, C., Barbarand, J., Ketcham, R.A., Tassan-Got, L., Van Der Beek, P., Pagel, M., Pinna-Jamme, R., Couffignal, F., Fialin, M., 2013. Chemical influence on α-recoil damage annealing in apatite: implications for (U-Th)/He dating. Chem. Geol. 351, 257–267. https://doi.org/10.1016/j.chemgeo.2013.05.027.

Grantz, A., May, S.D., Hart, P.E., 1990. Geology of the Arctic continental margin of Alaska. In: Grantz, A., Johnson, L., Sweeney, J.F. (Eds.), The Arctic Ocean Region. Geological Society of America, Geology of North America, Boulder, Colorado, pp. 257–288 v. L.

Green, P.F., Duddy, I.R., Gleadow, A.J.W., Tingate, P.R., Laslett, G.M., 1986. Thermal annealing of fission tracks in apatite 1. Variable temperature behaviour. Chem. Geol. Isot. Geosci. Sect. 59, 237–253. https://doi.org/10.1016/0168-9622(88)90019-X.

Guenthner, W.R., Reiners, P.W., Ketcham, R.A., Nasdala, L., Giester, G., 2013. Helium diffusion in natural zircon: radiation damage, anisotropy, and the interpretation of zircon (U-Th)/He thermochronology. Am. J. Sci. 313, 145–198. https://doi.org/10.2475/03.2013.01.

Guenthner, W.R., Reiners, P.W., DeCelles, P.G., Kendall, J., 2015. Sevier belt exhumation in central Utah constrained from complex zircon (U-Th)/He data sets: radiation damage and He inheritance effects on partially reset detrital zircons. Geol. Soc. Am. Bull. 127, 1–26. https://doi.org/10.1130/B31032.1.

Harrison, T.M., Zeitler, P.K., 2005. Fundamentals of noble gas thermochronometry. Rev. Mineral. Geochem. 58, 123–149. https://doi.org/10.2138/rmg.2005.58.5.

Ketcham, R.A., 2005. Forward and inverse modeling of low-temperature thermochronometry data. Rev. Mineral. Geochem. 58, 275–314. https://doi.org/10.2138/rmg.2005.58.11.

Ketcham, R.A., Carter, A., Donelick, R.A., Barbarand, J., Hurford, A.J., 2007. Improved modeling of fission-track annealing in apatite. Am. Mineral. 92, 799–810. https://doi.org/10.2138/am.2007.2281.

Kos'ko, M.K., Korago, E.A., 2009. Review of geology of the New Siberian Islands between the Laptev and the East Siberian Seas, northeast Russia. In: Stone, D.B., Fujita, K., Layer, P.W., Miller, E.L., Prokopiev, A.V., Toro, J. (Eds.), Geology, Geophysics and Tectonics of Northeasternb Russia: A Tribute to Leonid Parfenov. European Geosciences Union, Stephan Mueller Publication Series 4, pp. 45–64.

Kos'ko, M.K., Trufanov, G.V., 2002. Middle Cretaceous to Eopleistocene sequences on the New Siberian Islands: an approach to interpret offshore seismic. Mar. Petrol. Geol. 19, 901–919.

Kos'ko, M.K., Bondarenko, N.S., Nepomiluev, V.F., 1985. State Geological Map of the USSR, 1:200000 Scale. Sheets T-54-XXXI, XXXII, XXXIII; S-53-IV, V, VI, XI,XII; S-54-VII,VIII, IX, XIII, XIV, XV. Explanatory Note. Ministry of Geology, Moscow (in Russian).

Kośmińska, K., Majka, J., Manecki, M., Schneider, D.A., 2016. First Evidence of the Ellesmerian Metamorphism on Svalbard Geophysical Research Abstracts 18. EGU2016-12196, 2016 EGU General Assembly 2016 © Author(s) 2016. CC Attribution 3.0 License. .

Kuzmichev, A.B., 2009. Where does the South Anyui suture go in the New Siberian Islands

and Laptev Sea?: Implications for the Amerasia basin origin. Tectonophysics 463, 86–108.
Kuzmichev, A.B., Pease, V.L., 2007. Siberian trap magmatism on the New-Siberian islands: constraints for East Arctic Mesozoic plate tectonic reconstructions. J. Geol. Soc. Lond. 164, 959–968.
Kuzmichev, A.B., Aleksandrova, G.N., Herman, A.B., 2009. Aptian-Albian coaliferous sediments of Kotel'nyi Island (New Siberian Islands): new data on the section structure and ignimbrite volcanism. Stratigr. Geol. Correl. 17 (5), 69–94.
Kuzmichev, A.B., Aleksandrova, G.N., Herman, A.B., Danukalova, M.K., Simakova, A.N., 2013. Paleogene-neogene sediments of Bel'kov Island (New Siberian Islands): characteristics of sedimentary cover in the eastern Laptev shelf. Stratigr. Geol. Correl. 21 (4), 421–444.
Lane, L.S., 2007. Devonian-Carboniferous paleogeography and orogenesis, northern Yukon and adjacent Arctic Alaska. Can. J. Earth Sci. 44, 679–694.
Lawver, L.A., Grantz, A., Gahagan, L.M., 2002. Plate kinematic evolution of the present Arctic region since the Ordovician. In: Miller, E.L., Grantz, A., Klemperer, S.L. (Eds.), Tectonic Evolution of the Bering Shelf-Chukchi Sea-Arctic Margin and Adjacent Landmasses, Special Paper. Geological Society of America, Boulder, CO, pp. 333–358.
Layer, P.W., Parfenov, L.M., Surnin, A.A., Timofeev, V.F., 1993. First $^{40}Ar/^{39}Ar$ age determinations of magmatic and metamorphic rocks of the Verkhoyansk-Kolyma Mesozoides. Dokl. AN SSSR 329 (5), 621–624 (in Russian).
Layer, P.W., Newberry, R., Fujita, K., Parfenov, L.M., Trunilina, V.A., Bakharev, A.G., 2001. Tectonic setting of the plutonic belts of Yakutia, northeast Russia, based on 40Ar/39Ar geochronology and trace element geochemistry. Geology 29, 167–170.
Marrett, R.A., Allmendinger, R.W., 1990. Kinematic analysis of fault slip data. J. Struct. Geol. 12, 973–986.
Matushkin, N.Y., Metelkin, D.V., Vernikovsky, V.A., Travin, A.V., Zhdanova, A.I., 2016. Geology and age of mafic magmatism on Jeannette Island (De Long archipelago)—implications for paleotectonic reconstructions for the Arctic. Dokl. Earth Sci. 467 (1), 219–223.
McCann, A., 2000. Deformation of the Old Red Sandstone of NW Spitsbergen; links to the Ellesmerian and Caledonian orogenies. In: In: Friend, P.F., Williams, B.P.J. (Eds.), New Perspectives on the Old Red Sandstone. Geological Society, vol. 180. Special Publications, London, pp. 567–584.
Metelkin, D.V., Vernikovsky, V.A., Matushkin, N.Yu., Tolmacheva, T.Yu., Zhdanova, A.I., 2014. First paleomagnetic data for the Early Paleozoic deposits of New Siberian Islands: concerning the formation of the South Anyui Suture and tectonic reconstruction of Arctida. Litosfera 3, 11–31 (in Russian).
Metelkin, D.V., Vernikovsky, V.A., Matushkin, N.Yu., 2015. Arctida between Rodinia and Pangea. Precambrian Res. 259, 114–129.
Miller, E.L., Toro, J., Gehrels, G.E., Amato, J.M., Prokopiev, A., Tuchkova, M.I., Akinin, V.V., Dumitru, T.A., Moore, T.E., Cecile, M.P., 2006. New insights into Arctic paleogeography and tectonics from U–Pb detrital zircon geochronology. Tectonics 25 (TC3013), 19.
Natal'in, B.A., 1984. Early Mesozoic Eugeosyncline Systems of Northern Pacific Frame. Nauka, Moscow (in Russian).
Natal'in, B.A., Amato, J.M., Toro, J., Wright, J.E., 1999. Paleozoic rocks of Northern Chukotka Peninsula, Russian Far East: implications for the tectonics of the Arctic Region. Tectonics 18, 977–1003.
Nepomiluev, V.F., Preobrazhenskaya, E.N., Trufanov, G.V., et al., 1979. Lower Cretaceous rocks of the Kotel'nyi Island. Sov. Geol. 3, 104–109 (in Russian).
Nokleberg, W.J., Parfenov, L.M., Monger, J.W.H., Norton, I.O., Khanchuk, A.I., Stone, D.B., Scotese, C.R., Scholl, D.W., Fujita, K., 2001. Phanerozoic Tectonic Evolution of the Circum-North Pacific. U.S. Geological Survey Professional Paper 1626.
O'Brien, T.M., Miller, E.L., Benowitz, J.P., Meisling, K.E., Dumitru, T.A., 2016. Dredge samples from the Chukchi Borderland: implications for paleogeographic reconstruction and tectonic evolution of the Amerasia Basin of the Arctic. Am. J. Sci. 316 (9), 873–924. https://doi.org/10.2475/09.2016.03.
Parfenov, L.M., 1984. Continental Margins and Island Arcs of Mesozoides in Northeastern Asia. Nauka, Novosibirsk (in Russian).
Parfenov, L.M., Natapov, L.M., Sokolov, S.D., Tsukanov, N.V., 1993a. Terrane analysis and accretion in northeast Asia. Isl. Arc 2, 35–54.
Parfenov, L.M., Natapov, L.M., Sokolov, S.D., Tsukanov, N.V., 1993b. Terranes and accretionary tectonics of North-East Asia. Geotectonics 1, 68–78 (in Russian).
Parfenov, L.M., Kuz'min, M.I. (Eds.), 2001. Tectonics, Geodynamics and Metallogeny of the Sakha Republic (Yakutia). International Academic Publishing Company "Nauka/Interperiodica,", Moscow (in Russian).
Piepjohn, K., 2000. The Svalbardian-Ellesmerian deformation of the Old Red Sandstone and the pre-Devonian basement in NW Spitsbergen (Svalbard). In: In: Friend, P.F., Williams, B.P.J. (Eds.), New Perspectives on the Old Red Sandstone: Geological Society, vol. 180. Special Publications, London, pp. 585–601.
Piepjohn, K., von Gosen, W., Tessensohn, F., Saalmann, K., 2008. Ellesmerian fold-and-thrust belt (northeast Ellesmere Island, Nunavut) and its Eurekan overprint. Geol. Surv. Can. Bull. 592, 285–303.
Piepjohn, K., von Gosen, W., Tessensohn, F., Reinhardt, L., McClelland, W.C., Dallmann, W., Gaedicke, C., Harrison, J.C., 2015. Tectonic map of the Ellesmerian and Eurekan deformation belts on Svalbard, North Greenland, and the Queen Elizabeth Islands (Canadian Arctic). Arktos 12. https://doi.org/10.1007/s41063-015-0015-7.
Piepjohn, K., Lorenz, H., Franke, D., Brandes, C., von Gosen, W., Gaedicke, C., Labrousse, L., Sobolev, N.N., Solobev, P., Suan, G., Mrugalla, S., Talarico, F., Tolmacheva, T., 2017. Mesozoic structural evolution of the New Siberian Islands. In: In: Pease, V., Coakley, B. (Eds.), Circum-Arctic Lithosphere Evolution. Geological Society, vol. 460 Special Publications, London. https://doi.org/10.1144/SP460.1.
Prokopiev, A., Ershova, V., Sobolev, N., Kullerud, K., Khudoley, A., Ganerød, M., Petrov, E., 2017. New data on the timing of mafic magmatism in the New Siberian Islands from $^{40}Ar/^{39}Ar$ isotope dating. Abstract of AAPG2017 Conference.
Prokopiev, A.V., Ershova, V.B., Khudoley, A.K., Vasiliev, D.A., Baranov, V.V., Kalinin, M.A., 2018. Pre-mid-Frasnian angular unconformity on Kotel'ny Island (New Siberian Islands Archipelago): evidence of Mid-Paleozoic Deformation in the Russian High Arctic. Arctos. https://doi.org/10.1007/s41063-018-0059-6.
Reiners, P.W., Brandon, M.T., 2006. Using thermochronology to understand orogenic erosion. Annu. Rev. Earth Planet. Sci. 34, 419–466. https://doi.org/10.1146/annurev.earth.34.031405.125202.
Reiners, P.W., Farley, K.A., Hickes, H.J., 2002. He diffusion and (U-Th)/He thermochronometry of zircon: initial results from Fish Canyon Tuff and Gold Butte. Tectonophysics 349, 297–308. https://doi.org/10.1016/S0040-1951(02)00058-6.
Rippington, S., Scott, R.A., Smyth, H., Bogolepova, O., Gubanov, A., 2010. Calgary, Alberta, Canada, May 10–14, 2010The Ellesmerian Orogeny: Fact or Fiction? AAPG Search and Discovery Article #90172 © CSPG/CSEG/CWLS GeoConvention 20102010. The Ellesmerian Orogeny: Fact or Fiction? AAPG Search and Discovery Article #90172 © CSPG/CSEG/CWLS GeoConvention 2010. http://www.searchanddiscovery.com/pdfz/abstracts/pdf/2014/90172cspg/abstracts/ndx_rippi.pdf.html.
Samusin, A.I., Belousov, K.N., 1985. State Geological Map of the USSR, Scale 1: 200000. New Siberian Islands Series. Sheets S-53-XVI, XVII, XXIII; S-54-XIV–XVI, XX–XXVII, XXVII–XXX. Explanatory Notes. Soyuzgeolfond, Moscow (in Russian). .
Sengo¨r, C., Natal'in, B., 1996. Palaeotectonics of Asia: fragments of a synthesis. In: Yin, A., Harrision, M. (Eds.), The Tectonic Evolution of Asia. Cambridge University Press, Cambridge, pp. 486–640.
Seslavinsky, K.B., 1979. South-Anyui suture (Western Chukotka). Trans. (Dokl.) Russ. Akad. Sci. 249, 1181–1185 (in Russian).
Shephard, G.E., Müller, R.D., Seton, M., 2013. The tectonic evolution of the Arctic since Pangea breakup: integrating constraints from surface geology and geophysics with mantle structure. Earth. Rev. 124, 148–183.
Shuster, D.L., Flowers, R.M., Farley, K.A., 2006. The influence of natural radiation damage on helium diffusion kinetics in apatite. Earth Planet. Sci. Lett. 249, 148–161. https://doi.org/10.1016/j.epsl.2006.07.028.
Sobolev, N.N., Metelkin, D.V., Vernikovsky, V.A., Matushkin, N.Y., Prokopiev, A.V., Ershova, V.B., Shmanyak, A.V., Petrov, E.O., 2014. The first information about the geology of the Jeannette island (De Long Islands, the New Siberian Islands). Dokl. Earth Sci. 459 (5), 595–600.
Sokolov, S.D., Bondarenko, G.Ye, La yer, P.W., Kravchenko-Berezhnoy, I.R., 2009. South Anyui suture: tectono-stratigraphy, deformations, and principal tectonic events. In: In: Stone, D.B., Fujita, K., Layer, P.W., Miller, E.L., Prokopiev, A.V., Toro, J. (Eds.), Geology, Geophysics and Tectonics of Northeastern Russia: A Tribute to Leonid Parfenov, European Geosciences Union, vol. 4. Stephan Mueller Publication Series, pp. 201–221.
Sokolov, S.D., Tuchkova, M.I., Ganelin, A.V., Bondarenko, G.E., Layer, P., 2015. Tectonics of the South Anyui suture, Northeastern Asia. Geotectonics 49 (1), 3–26.
Soper, N.J., Higgins, A.K., 1990. Models for the Ellesmerian mountain front in North Greenland: a basin margin inverted by basement uplift. J. Struct. Geol. 12 (1), 83–97.
Spektor, V.B., Andrusenko, A.M., Dudko, E.A., Kareva, N.F., 1981. Continuation of the South-Anyui suture in the Primorsky lowland. Trans. (Dokl.) Russ. Akad. Sci. 260, 1447–1450 (in Russian).
Trufanov, G.V., Belousov, K.N., Nepomiluev, V.F., 1986. State Geological Map of the USSR. Scale 1:200000. Series New-Siberian islands. Sheets T-54-XXXIV, XXXV, XXXVI; T-56-XXXIII; S-54-IV,V,VI,X,XI,XII; S-55-I,II,III,IV,V,VI,VII,VIII,IX,X,XI,XII; S-56-III,VII. Explanatory Notes. Soyuzgeolfond, Moscow (in Russian).
Vernikovsky, V.A., Metelkin, D.V., Tolmacheva, T.Yu., Malyshev, N.A., Petrov, O.V., Sobolev, N.N., Matushkin, N.Yu., 2013. Concerning the issue of paleotectonic reconstructions in the Arctic and of the tectonic unity of the New Siberian Islands Terrane: new paleomagnetic and paleontological data. Dokl. Earth Sci. 451 (2), 791–797.
Verzhbitsky, V.E., 2004. On the Cretaceous – Cenozoic tectonic evolution of Eastern Laptev Sea Region (mesostructural data from Bel'kov Island, Russian Arctic). Abstracts of the 32nd International Geological Congress (Florence-Italy, Aug. 20–28, 2004) 1 p. 269.
Verzhbitsky, V.E., 2009. Folded complexes of Bel'kovsky Island: present-day structure and stages of development of eastern part of Laptev Sea region. EAGE «Geomodel – 2009» (in Russian).
Verzhbitsky, V.E., Sokolov, S.D., Tuchkova, M.I., Lobkovsky, L.I., 2014. New data on the structure and tectonic evolution of Wrangel Island (Russian East Arctic). Dokl. Earth Sci. 456 (2), 672–676.
Verzhbitsky, V.E., Sokolov, S.D., Tuchkova, M.I., 2015. Present day structure and stages of tectonic evolution of Wrangel Island, Russian Eastern Arctic Region. Geotektonika 3, 3–35. https://doi.org/10.1134/S001685211503005X. (in Russian).
Vinogradov, V.A., Kameneva, G.I., Yavshitz, G.P., 1975. On the Hyperborean Platform with respect to the new data on the geology of the Henrietta Island. Tectonics of the Arctic 1. NIIGA, Leningrad, pp. 21–25 (in Russian).
Wolfe, M.R., Stockli, D.F., 2010. Zircon (U–Th)/He thermochronometry in the KTB drill hole, Germany, and its implications for bulk He diffusion kinetics in zircon. Earth Planet. Sci. Lett. 295, 69–82. https://doi.org/10.1016/j.epsl.2010.03.025.
Zonenshain, L.P., Kuzmin, M.I., Natapov, L.M., 1990. In: In: Page, B.M. (Ed.), Geology of the USSR: A Plate Tectonic Synthesis. Geodynamics Series, vol. 21 American Geophysical Union, Washington, D.C 242 pp.